DOI: 10.1002/chem.200600989

Design and Synthesis of Binucleating Macrocyclic Clefts Derived from Schiff-Base Calixpyrroles

Gonzalo Givaja,[a] Manuel Volpe,[a] James W. Leeland,[a] Michael A. Edwards,[a] Thomas K. Young,[a] S. Barnie Darby,[a] Stuart D. Reid,[a] Alexander J. Blake,[a] Claire Wilson,[a] Joanna Wolowska,[b] Eric J. L. McInnes,[b] Martin Schröder,[a] and Jason B. Love*[a]

Abstract: The syntheses, characterisation and complexation reactions of a series of binucleating Schiff-base calixpyrrole macrocycles are described. The acid-templated [2+2] condensations between *meso*-disubstituted diformyldipyrromethanes and *o*-phenylenediamines generate the Schiff-base pyrrolic macrocycles $H_4\mathbf{L^1}$ to $H_4\mathbf{L^6}$ upon basic workup. The single-crystal X-ray structures of both $H_4\mathbf{L^3}\cdot 2\,EtOH$ and $H_4\mathbf{L^6}\cdot H_2O$ confirm that [2+2] cyclisation has occurred, with either EtOH or H_2O hydrogen-bonded within the macrocyclic cleft. A series of complexation reactions generate the dipalladium $[Pd_2(\mathbf{L})]$ ($\mathbf{L}=\mathbf{L^1}$ to $\mathbf{L^5}$), dinickel $[Ni_2(\mathbf{L^1})]$ and dicopper $[Cu_2(\mathbf{L})]$ ($\mathbf{L}=\mathbf{L^1}$ to $\mathbf{L^3}$) complexes. All of these complexes have been structurally characterised in the solid state and are found to adopt wedged structures that are enforced by the rigidity of the aryl backbone to give a cleft reminiscent of the structures of Pacman porphyrins. The binuclear nickel complexes $[Ni_2(\mu\text{-}OMe)_2Cl_2(HOMe)_2(H_4\mathbf{L^1})]$ and $[Ni_2(\mu\text{-}OH)_2Cl_2(HOMe)(H_4\mathbf{L^5})]$ have also been prepared, although in these cases the solid-state structures show that the macrocyclic ligand remains protonated at the pyrrolic nitrogen atoms, and the Ni^{II} cations are therefore co-ordinated by the imine nitrogen atoms only to give an open conformation for the complex. The dicopper complex $[Cu_2(\mathbf{L^3})]$ was crystallised in the presence of pyridine to form the adduct $[Cu_2(py)(\mathbf{L^3})]$, in which, in the solid state, the pyridine ligand is bound within the binuclear molecular cleft. Reaction between $H_4\mathbf{L^1}$ and $[Mn(thf)\{N(SiMe_3)_2\}_2]$ results in clean formation of the dimanganese complex $[Mn_2(\mathbf{L^1})]$, which, upon crystallisation, formed the mixed-valent complex $[Mn_2(\mu\text{-}OH)(\mathbf{L^1})]$ in which the hydroxo ligand bridges the metal centres within the molecular cleft.

Keywords: EPR spectroscopy · macrocyclic ligands · metallation · N ligands · transition metals

Introduction

While the physical properties and reactivity patterns of mononuclear transition metal complexes are controlled precisely by using design features intrinsic to the supporting ligand set, the inclusion of more than one metal centre introduces additional synthetic challenges, as both the local co-ordination spheres and respective locations of the metal centres must be defined. Moreover, important chemical transformations, such as alkane oxygenation,[1] oxygen reduction,[2,3] redox reactions involving hydrogen,[4] and nitrogen fixation,[5] are efficiently mediated by metalloenzymes that contain bi- or multimetallic reactive sites that are precisely organised by attendant ligands and an associated protein envelope.[6] Thus, the design and exploitation of ligands that can promote the construction of bi- and multimetallic complexes that imitate or surpass enzymes as catalysts in

[a] Dr. G. Givaja, Dr. M. Volpe, J. W. Leeland, M. A. Edwards, T. K. Young, S. B. Darby, S. D. Reid, Dr. A. J. Blake, Dr. C. Wilson, Prof. M. Schröder, Dr. J. B. Love
School of Chemistry
University of Nottingham
University Park
Nottingham, NG72RD (UK)
Fax: (+44) 115-951-3563
E-mail: jason.love@nottingham.ac.uk

[b] Dr. J. Wolowska, Dr. E. J. L. McInnes
EPSRC Multi-frequency EPR Service
School of Chemistry, University of Manchester
Oxford Road, Manchester, M139PL (UK)

Supporting information for this article is available on the WWW under http://www.chemeurj.org/ or from the author.

such processes have both a long-held fascination and strategic significance.[7] This design strategy is exemplified by the synthesis and chemistry of cofacial diporphyrin complexes, in which the well-known co-ordinative properties of the porphyrin are combined with exceptional control of the intermetallic separation by a rigid and well-defined spacer between the two porphyrinic compartments (see Scheme 1).[8,9]

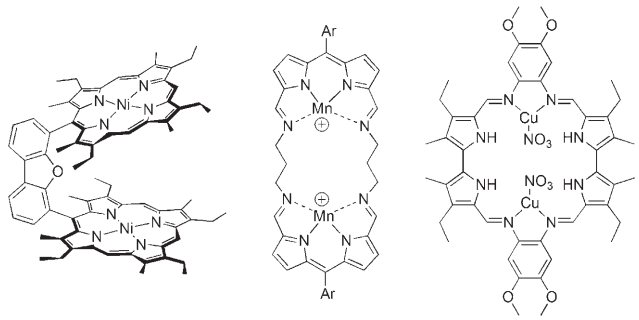

Scheme 1. Examples of binuclear transition metal complexes of cofacial diporphyrins and Schiff-base expanded porphyrin macrocycles.[20,45,61]

The resultant bimetallic molecular cleft facilitates extensive stoichiometric and catalytic small-molecule chemistry, such as oxygen redox and atom-transfer reactions,[3,10] hydrogen activation,[11,12] nitrogen reduction[13] and alkane activation.[11,14] Furthermore, it is possible to vary the two cofacial donor compartments to form porphyrin-corroles and bis(corrole) binuclear complexes; these compounds also catalyse oxygen reduction.[15,16] Other classes of polypyrrolic ligands, such as expanded porphyrins, have also been exploited in the formation of binuclear complexes, and, in contrast to cofacial diporphyrins, generally result in metal compounds that have flattened structures due to extensive π conjugation of the porphyrinic macrocycle.[17]

In an effort to provide more co-ordinative flexibility and modularity of design, and also to surmount the sometimes arduous synthetic routes to cofacial and expanded porphyrins, focus has shifted to the development of Schiff-base porphyrin analogues as binucleating ligands for transition metals.[18] Significantly, this class of macrocyclic ligand combines the desired co-ordinative features of the pyrrole group with the exceptional design characteristics and synthetic versatility of Schiff-base condensation procedures that can assist in ligand synthesis and engender structural control in the resultant bimetallic complexes. Condensation reactions between 2,2′-5,5′-diformyldipyrromethenes and aliphatic diamines have been shown to result in the formation of [2+2] accordion diporphyrins in which the two N_4-iminopyrrole donor compartments are separated by an alkyl linker (Scheme 1).[19–21] However, the flexibility of this linking chain results in bimetallic complexes in which the relative positions of the metal centres are not well defined; even so, such dimanganese complexes do act as catalysts for the reduction of peroxide.[19] Alternatively, [2+2] Schiff-base calixpyrroles formed from the condensation of 2,2′-5,5′-diformylbipyrroles with *o*-diaminobenzenes generate bimetallic complexes similar to those of expanded porphyrins in which more rigid and flattened structures are adopted due to more extensive π conjugation (Scheme 1).[20]

Using standard Vilsmeier–Haack formylation procedures, we[22] and others[23] have recently developed synthetic pathways to the 2,2′-5,5′-diformyldipyrromethanes **i** and **ii** (Scheme 2). We have shown that these synthons react with primary amines to form new acyclic iminopyrrole ligands that support the formation of binuclear [4+4] double helicates of Mn^{II}, Fe^{II} and Co^{II} that display asymmetric, binuclear cleft motifs in the solid state.[24,25] It was clear to us that condensation of **i** or **ii** with *o*-diaminobenzenes should result in the formation of [2+2] Schiff-base calixpyrroles (Scheme 2), and that these macrocycles would afford binuclear transition metal complexes. Furthermore, we reasoned that the combination of the two N_4-iminopyrrole donor compartments linked by rigid aryl spacers should result in complexes of well-defined structure. We report herein the syntheses and characterisation of a series of Schiff-base calixpyrrole macrocycles H_4**L**, which form binuclear complexes that adopt molecular cleft structures similar to those of cofacial or Pacman diporphyrins; some of this work has been previously communicated.[26] Sessler and co-workers have reported independently routes to the Schiff-base calixpyrrole H_4**L**^{1} and its analogues and have shown that binuclear $Fe^{III}_2(\mu\text{-O})$, Cu^{I}_2 and Cu^{II}_2 motifs can be supported by this ligand.[27–29] Furthermore, Brooker and co-workers have exploited dipyrromethane synthon **i** for the metal-templated syntheses of macrocycles analogous to H_4**L**. These ionophores incorporate flexible alkyl-chain spacers between the N_4-donor compartments, and their binuclear complexes therefore adopt flattened structures similar to accordion diporphyrins.[30]

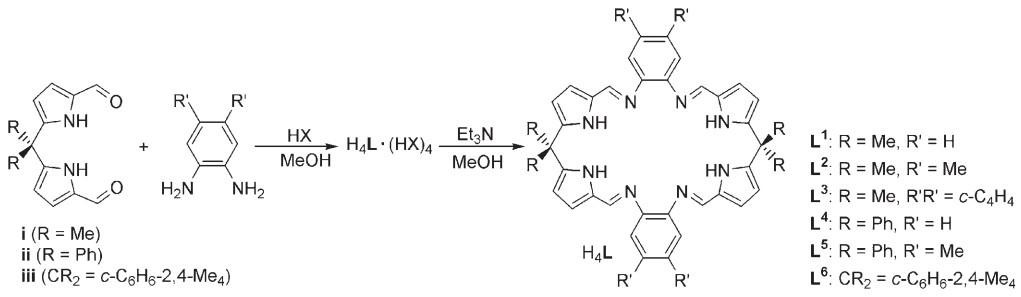

Scheme 2. Synthesis of the Schiff-base calixpyrrole macrocycles H_4**L**^{1}–H_4**L**^{6} (**L**^{1} to **L**^{5}, HX = HOTs; **L**^{6}, HX = HO_2CCF_3).

Results and Discussion

Ligand synthesis and structure: *meso*-Disubstituted diformyldipyrromethanes **i** and **ii** react with aromatic *o*-disubstituted diamines in MeOH in the presence of TsOH to generate the orange and crystalline [2+2] macrocyclic products $H_4\mathbf{L^1}(TsOH)_4$ in good yield (Scheme 2). The use of acid as a template in these reactions is the key, and, as described independently by Sessler and co-workers, a variety of acids can mediate this [2+2] cyclisation reaction.[29]

The ^{1}H NMR spectrum of $H_4\mathbf{L^1}(TsOH)_4$ shows a single resonance characteristic of imine formation at $\delta = 8.53$ ppm plus AB doublets at $\delta = 7.32$ and 7.01 ppm that integrate as four arylsulfonic acid groups per macrocycle, that is, each imine nitrogen atom is protonated, in contrast to the synthesis of $H_4\mathbf{L^1}(HCl)_2$, in which the macrocycle is doubly protonated.[29] Treatment of these acid salts with a base such as NaOH or Et_3N in alcoholic solvents quantitatively precipitates the acid-free macrocycles $H_4\mathbf{L}$ ($\mathbf{L} = \mathbf{L^1}$–$\mathbf{L^6}$), which can be isolated simply by suction filtration. These yellow, air-stable, amorphous materials are poorly soluble in common organic solvents unless additional protic solvent is present; presumably, in the absence of protic solvents, these macrocycles form hydrogen-bonded aggregates in the solid state. The ^{1}H NMR spectrum of $H_4\mathbf{L^1}$ in a mixture of $CDCl_3$ and [D_4]methanol confirms the absence of the tosylate anion and retention of the imine group, associated with a singlet resonance at $\delta = 8.07$ ppm; no resonances due to the pyrrolic NH groups are observed due to rapid exchange with the protic solvent. While neutralisation reactions in methanolic solution result in amorphous powders, we discovered that yellow, crystalline macrocycles $H_4\mathbf{L}\cdot n$EtOH are deposited from hot ethanol. The solid-state structure of $H_4\mathbf{L^3}\cdot 2$EtOH, the macrocycle derived from 1,2-diaminonaphthalene and **i**, was determined, and is shown in Figure 1; selected bond lengths and angles are listed in Table 1. The crystal structure of $H_4\mathbf{L^3}\cdot 2$EtOH confirms that [2+2] cyclisation has taken place, and that a neutral macrocycle is formed on addition of Et_3N to the acid salt.

Table 1. Selected bond lengths [Å] and angles [°] for $H_4\mathbf{L^3}\cdot 2$EtOH and $H_4\mathbf{L^6}\cdot H_2O$.

	$H_4\mathbf{L^3}\cdot(EtOH)_2$	$H_4\mathbf{L^6}\cdot(H_2O)$
N1–C1	1.2824(17)	1.289(3)
N1–C46	1.4091(17)	–
N1–C26A	–	1.413(3)
C1–C2	1.4313(19)	1.433(3)
C2–C3	1.3729(19)	1.371(3)
N2–C2	1.3752(17)	1.375(3)
N2–C5	1.3602(16)	1.370(3)
C3–C4	1.405(2)	1.400(3)
C4–C5	1.3739(19)	1.383(3)
C1-N1-C46	120.66(13)	–
C1-N1-C26A	–	121.0(3)

The Schiff-base calixpyrrole adopts a non-linear, bowl-like conformation around a hydrogen-bonded molecule of EtOH, but the second molecule of EtOH does not interact with the macrocyclic ligand. The presence of co-ordinated EtOH within the macrocyclic cavity illustrates the capacity of $H_4\mathbf{L^3}$ to act both as a hydrogen-bond donor, through interactions between pyrrole NH protons and the ethanolic oxygen atom (N2···O1 2.992, N7···O1 2.960 Å), and as a hydrogen-bond acceptor, through interactions between the imine N atoms and the ethanolic OH proton (N8···O1 2.990, N1···O1 3.001 Å). These hydrogen-bonding interactions are commensurate with the development of similar Schiff-base calixpyrroles and acyclic iminopyrrole compounds as effective anion-binding agents.[31] The non-linear structure adopted by $H_4\mathbf{L^3}$ is unlike that seen for related expanded porphyrins and Schiff-base porphyrin analogues, and is a consequence of both conformational flexibility and the lack of extended π conjugation that results from the incorporation of sp^3-hybridised *meso*-CMe_2 groups into the macrocyclic framework. It is clear from the solid-state structure of $H_4\mathbf{L^3}$ that the *meso*-CMe_2 groups can act as a hinge that effectively compartmentalises two N_4-donor sets.

We have also determined the X-ray crystal structure of $H_4\mathbf{L^6}$, a macrocycle that incorporates bulky *meso*-tetramethylcyclohexyl substituents (see Figure 1, Table 1). In a similar manner to $H_4\mathbf{L^3}$, this macrocycle adopts a wedge-shaped conformation due to hydrogen-bonding donor and acceptor interactions between pyrrole and imine nitrogen atoms and a molecule of water (O1W···N1 3.127, O1W···N2 3.109, O1W···N3 3.197, O1W···N4 3.243 Å). However, unlike in $H_4\mathbf{L^3}$, this introduces a hinge into the macrocycle at the *o*-aryl groups, which results in the formation of a hinged cleft structural motif. Thus, two distinctly different structural motifs are formed by this ligand framework, and are therefore expected to result in different metal-binding N_4-donor compartments.

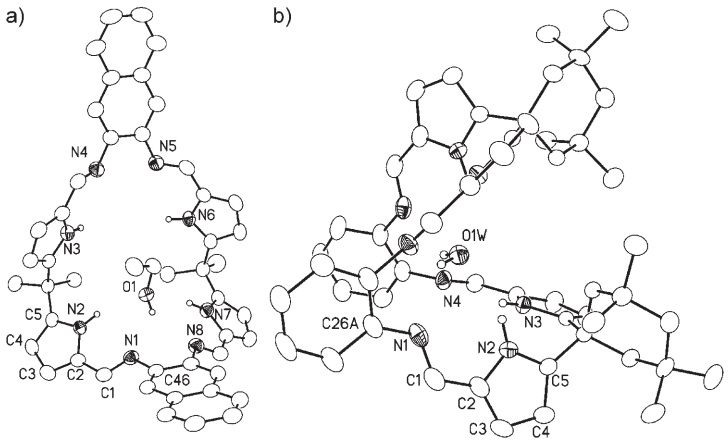

Figure 1. Solid-state structures of a) $H_4\mathbf{L^3}\cdot 2$EtOH and b) $H_4\mathbf{L^6}\cdot H_2O$. For clarity, all hydrogen atoms, except those involved in hydrogen bonding, and solvent molecules have been removed for clarity (50% probability displacement ellipsoids).

The structure of $H_4\mathbf{L^3}$ was examined in solution by variable-temperature

^{1}H NMR spectroscopy, with and without added [D_4]methanol solvent (see Supporting Information). Similarly large cyclopolypyrroles, such as cycloocta- and cyclododecapyrrole, exhibit dynamic behaviour in solution; on cooling to low temperature, the ^{1}H NMR spectra of these macrocycles correlate well to their "looped" solid-state structures.[32] Cooling a solution of anhydrous $H_4\mathbf{L^3}$ in [D_8]THF to 183 K results in no significant change to the ^{1}H NMR spectrum, other than line broadening at low temperatures. However, the addition of a small amount of [D_4]methanol to the sample caused the ^{1}H NMR resonances to sharpen considerably at room temperature and, between 233 and 203 K, results in broadening of the resonance associated with the *meso*-CH_3 protons and its decoalescence into two new signals that overlap considerably with the resonance of residual THF at $\delta = 1.73$ ppm; the remaining ligand resonances remain unaffected. This dynamic behaviour is consistent with the adoption of a hinged, C_2-symmetric macrocyclic conformation at low temperature in which the *meso*-methyl groups are oriented *endo* and *exo* to a macrocyclic cleft, and is presumably promoted by hydrogen-bonding interactions with the protic solvent, as observed in the structures of $H_4\mathbf{L^3}\cdot 2\,EtOH$ and $H_4\mathbf{L^6}\cdot H_2O$ (see above). Indeed, this solution structure correlates to both of the wedged solid-state structures of $H_4\mathbf{L^3}$ and $H_4\mathbf{L^6}$ if, in the former structure, it is assumed that the hydrogen-bonded EtOH molecule can shuttle between the two N_4 compartments at low temperature. Whereas this organisation of the ligand framework into a predefined, wedged conformation in protic solvents is observed only at low temperature, the predisposition for such an organised ligand structure in solution may well influence the formation and structural behaviour of the metal complexes of **L**.

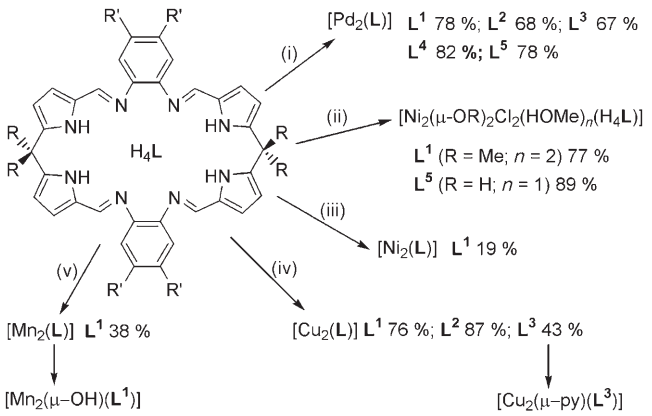

Scheme 3. Synthesis of transition metal complexes of **L**. Conditions: i) $Pd(OAc)_2$, NEt_3, CH_2Cl_2; ii) $NiCl_2\cdot 6H_2O$, CH_2Cl_2/MeOH, NEt_3; iii) a) KH; b) [$NiCl_2$(dme)], THF, Δ; iv) $Cu(BF_4)_2\cdot x H_2O$, NEt_3, CH_2Cl_2; v) [$Mn(thf)_2\{N(SiMe_3)_2\}_2$] PhMe, Δ.

Palladium complexes: The reactions between $Pd(OAc)_2$, Et_3N and $H_4\mathbf{L}$ ($\mathbf{L} = \mathbf{L^1}$ to $\mathbf{L^5}$) in CH_2Cl_2 at ambient temperature result in the formation of the red binuclear palladium complexes [$Pd_2(\mathbf{L})$] in good yields (Scheme 3). Electrospray mass spectra of the reaction mixtures show the molecular ions $[Pd_2(\mathbf{L})]^+$ with appropriate isotopic patterns and are consistent with the sole formation of the Pd^{II} complexes; elemental analyses also support the proposed molecular formula and indicate that the five dimetallic complexes are neutral with no counterions. The absorptions at 1557 and 1561 cm^{-1} observed for [$Pd_2(\mathbf{L^1})$] and [$Pd_2(\mathbf{L^3})$] in their respective IR spectra are attributable to imine/pyrrole ν(C=N) stretching vibrations. The electronic spectrum of [$Pd_2(\mathbf{L^1})$] in $CHCl_3$ shows intense absorptions at $\lambda = 311$ ($\lg\varepsilon = 4.56$), 414 ($\lg\varepsilon = 4.35$) and 433 nm ($\lg\varepsilon = 4.35$), similar to the diagnostic Soret and Q-bands observed in the electronic spectra of porphyrinic complexes, albeit of reduced intensity and blue-shifted.

Structural characterisation of [$Pd_2(\mathbf{L})$]: Crystals suitable for X-ray diffraction were obtained for the dipalladium complexes, and their structures determined; selected bond lengths and angles are listed in Table 2. The overall structur-

Table 2. Selected bond lengths [Å] and angles [°] for [$Pd_2(\mathbf{L})$] ($\mathbf{L} = \mathbf{L^2}$, $\mathbf{L^3}$, $\mathbf{L^5}$), [$Ni_2(\mathbf{L^1})$], [$Cu_2(\mathbf{L})$] ($\mathbf{L} = \mathbf{L^1}$, $\mathbf{L^2}$, $\mathbf{L^3}$) and [$Cu_2(\mu$-py)($\mathbf{L^3}$)] complexes.

	[$Pd_2(\mathbf{L^2})$]	[$Pd_2(\mathbf{L^3})$]	[$Pd_2(\mathbf{L^5})$]	[$Ni_2(\mathbf{L^1})$]	[$Cu_2(\mathbf{L^1})$]	[$Cu_2(\mathbf{L^2})$]	[$Cu_2(\mathbf{L^3})$]	[Cu_2(py)($\mathbf{L^3}$)]
M1−N1	2.068(4)	2.049(2)	2.068(8)	1.938(2)	2.004(4)	1.987(2)	1.996(2)	2.067(3)
M1−N2	1.935(4)	1.937(2)	1.920(10)	1.827(2)	1.915(3)	1.919(2)	1.915(2)	1.948(3)
M1−N3	1.928(4)	1.934(2)	1.935(9)	1.814(2)	1.893(4)	1.903(2)	1.897(2)	1.933(3)
M1−N4	2.059(4)	2.096(2)	2.058(10)	1.921(2)	2.045(3)	2.073(3)	2.050(2)	2.090(3)
M2−N5	2.051(4)	2.049(2)	2.060(10)			1.990(2)	1.987(2)	2.008(3)
M2−N6	1.947(4)	1.937(2)	1.945(9)			1.911(2)	1.920(2)	1.906(3)
M2−N7	1.935(4)	1.937(2)	1.928(10)			1.891(3)	1.903(2)	1.904(3)
M2−N8	2.075(4)	2.078(2)	2.081(9)			2.039(2)	2.084(2)	2.012(3)
M1−N9								2.258(3)
M2−N9								2.983
N1-M1-N2	80.32(19)	79.94(9)	80.2(4)	83.67(10)	81.98(15)	81.54(10)	81.39(10)	81.08(12)
N2-M1-N3	88.4(2)	88.18(9)	88.2(4)	88.40(10)	86.52(15)	86.51(11)	86.41(10)	84.80(13)
N3-M1-N4	80.03(17)	80.68(9)	81.4(4)	83.21(10)	82.48(15)	82.84(10)	82.36(10)	81.21(12)
N1-M1-N4	111.27(17)	110.99(8)	110.3(4)	104.95(10)	109.00(14)	109.49(10)	109.72(9)	106.13(12)
N5-M2-N6	80.26(17)	79.96(9)	80.4(4)			81.65(10)	81.44(10)	82.59(13)
N6-M2-N7	88.01(17)	88.26(9)	88.4(4)			87.41(11)	87.50(10)	85.72(13)
N7-M2-N8	80.43(17)	80.65(9)	81.3(4)			82.61(10)	82.11(10)	82.82(12)
N8-M1-N5	111.29(16)	110.93(8)	109.9(4)			108.13(10)	108.66(9)	108.55(12)
M1−N9···M2								99.08

al characteristics of these compounds are similar, so only [Pd_2($\mathbf{L^3}$)] will be discussed in detail; the X-ray crystal structures of [Pd_2($\mathbf{L^1}$)] and [Pd_2($\mathbf{L^4}$)] have been reported previously by us.[26]

In [Pd_2($\mathbf{L^3}$)] (Figure 2), each Pd^{II} cation is bound to two deprotonated pyrrole nitrogen atoms of one dipyrromethane unit and to the two adjoining imine nitrogen donor atoms in an N_4 co-ordination sphere. The metal centres adopt square-planar geometries (sum of angles at Pd1 359.79, Pd2 359.80°), in which Pd1 is located 0.048 Å out of the mean plane (o.o.p) defined by the N_4 donor atoms, whereas Pd2 is 0.071 Å o.o.p. Two distinct sets of Pd–N bond lengths are observed, shorter (av 1.936 Å) to the pyrrolic nitrogen atoms (N2 N3, N6, N7) and longer (av 2.068 Å) to the four imine nitrogen atoms (N1, N4, N5, N8). The N-Pd-N angles range from 79.94(9) to 110.989(8)°, the smallest angle being defined by the pyrrole-imine chelate and the largest involving both imine nitrogen atoms. The presence of the sp^3-hybridised *meso*-CMe_2 link between the planar imine-pyrrole chelates not only limits electronic conjugation of the macrocycle, but also introduces a degree of flexibility within the complex. Thus, the imine-pyrrole chelates are not coplanar, and display dihedral angles between $Pd1N_4$ and $Pd2N_4$ compartments of 11.0 and 19.7°, respectively. Importantly, the metal–ligand geometry, together with the presence of the rigid *o*-aryl spacers between the two PdN_4-donor compartments, has a significant impact on the overall molecular shape of [Pd_2($\mathbf{L^3}$)]. This results in a dimetallic molecular cleft structure in which the *o*-aryl units are offset, face-to-face π-stacked (intrastack distance 3.604 Å, offset angle 23°)[33] and act as hinges that promote a wedgelike arrangement of the two PdN_4 square planes. This gross structural motif is similar to those observed for single-pillared or Pacman diporphyrin complexes,[9] in which the spatial separation between two metal porphyrins is rigidly defined by an appropriate, generally aromatic, spacer unit. The structure of [Pd_2($\mathbf{L^3}$)] can be compared to those of similar molecules by defining three variables: the metal–metal separation (M···M) and the "bite" (θ) and torsional twist (Φ) angles between the two MN_4 compartments (see Figure 3); these have been determined for all of the structurally characterised complexes described here and are detailed in Table 3.

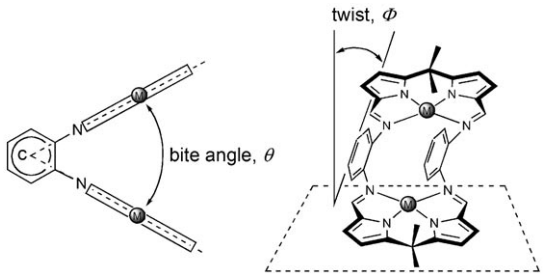

Figure 3. Schematic showing the definition of the bite angle θ (θ = M-C-M angle, C = bisector of the vector between the aryl ring centroids) and torsional twist Φ (Φ = normal dihedral angle of MN_4 and aryl C_6 plane).

The effect of varying the substituents at the *meso*-carbon atom or at the 3,4-positions of the *o*-aryl hinge can be analysed by comparing the structures of the dipalladium complexes [Pd_2($\mathbf{L}$)]. The Pd···Pd separation varies between 3.544 and 4.120 Å, and, in contrast to Pacman diporphyrinic analogues in which the M···M separation can vary between 3.5 and 7.8 Å (this range is dependant on the nature of the spacer in the Pacman ligand),[34] represents a small and rigidly constrained vertical translation. Furthermore, the X-ray crystal structures of the dipalladium Pacman bis-porphyrin complexes [Pd_2(DPX)] and [Pd_2(DPD)], where DPX and DPD are dibenzoxanthene and dibenzofuran pillars, respectively, show cofacial arrangements of the porphyrins [bite angles: 3.9 (DPX) and 11.0° (DPD); torsional twists: 14.6 (DPX) and 3.5° (DPD)], with considerably different Pd···Pd separations [3.97 (DPX) and 6.81 Å (DPD)].[35] The palladium complexes [Pd_2($\mathbf{L}$)] can also be compared to Pacman diporphyrins that were synthesised by Naruta and co-workers, in which the two porphyrins are linked by a similar *o*-phenylene spacer.[36–38] In contrast to [Pd_2($\mathbf{L}$)], *meso*-mesityl-substituted dicobalt complexes of these ligands adopt wedged-geometries with large intermetallic separations (e.g., 6.570(2) Å),[37] while dizinc analogues are truly cofacial and display short interplanar separations (3.43 Å) due to favourable π-stacking interactions.[39] The intermetallic separation in the [Pd_2($\mathbf{L}$)] complexes appears to be intrinsically linked to both the bite and twist angles, which are dependant on ligand substitution patterns. Better offset, face-to-face π-stacking overlap of the hinge

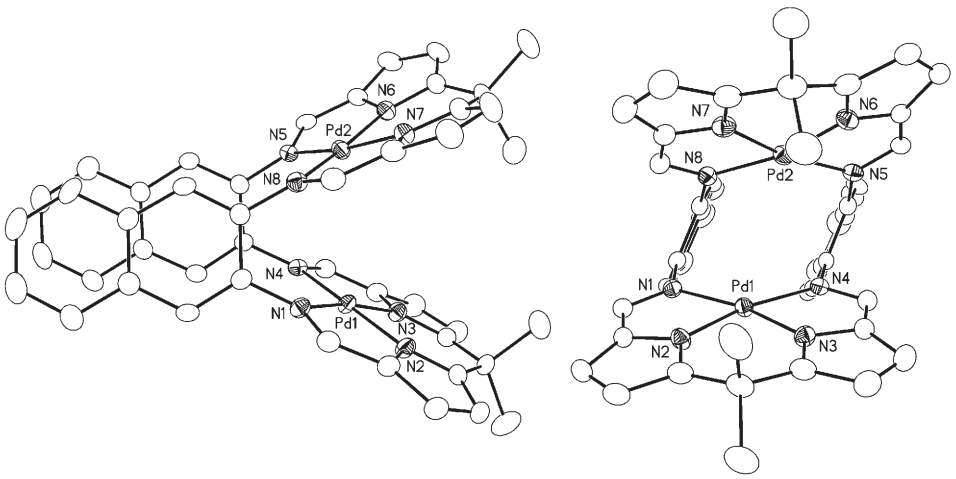

Figure 2. Solid-state structure of [Pd_2($\mathbf{L^3}$)] (50% displacement ellipsoids). For clarity, solvent molecules and all hydrogen atoms are omitted.

Table 3. Comparison of the geometric data of Pd, Ni, Cu, Mn and Fe Pacman complexes of **L**.

Compound	Twist [°][a]	Bite [°][a]	M···M [Å]	Ref.
$[Pd_2(\mathbf{L^1})]$	18.8	56.5	3.762	[26]
$[Pd_2(\mathbf{L^2})]$	11.1	62.1	4.108/4.120[b]	this work
$[Pd_2(\mathbf{L^3})]$	23.0	53.0	3.544	this work
$[Pd_2(\mathbf{L^4})]$	21.6	57.4	3.828	[26]
$[Pd_2(\mathbf{L^5})]$	28.5	59.7	3.944	this work
$[Pd_2(DPX)]$	14.6	3.9	3.97	[35]
$[Ni_2(\mathbf{L^1})]$	30.3	54.9	3.632	this work
$[Ni_2(DPX)]$	22.2	1.9	4.689	[45]
$[Cu_2(\mathbf{L^1})]$	26.2	61.0	4.014	this work
$[Cu_2(\mathbf{L^1})]$	24.0	52.1	3.473	[27][c]
$[Cu_2(\mathbf{L^1})]$	20.5	62.0	4.053	[27][c]
$[Cu_2(\mathbf{L^2})]$	28.3	53.4	3.695/3.738[b]	this work
$[Cu_2(\mathbf{L^3})]$	32.2	53.3	3.552	this work
$[Cu_2(\mu\text{-py})(\mathbf{L^3})]$.	19.6	59.9	4.014	this work
$[Cu_2(DPX)]$	7.4	2.3	3.910	[45]
$[Mn_2(\mu\text{-OH})(\mathbf{L^1})]$	4.9	49.7	3.417	this work
$[Fe_2(\mu\text{-O})(\mathbf{L^1}]$	0.3	44.8	3.145	[28][c]

[a] The twist angle was calculated as the dihedral angle between the backbone C_6 aryl and MN_4 planes (i.e., 0° = no twist), and the bite angle was determined as the M-X-M angle, where X = bisector of the centroid–centroid vector of the backbone C6 aryl rings (see Figure 3). [b] Two molecules in the asymmetric unit. [c] Determined from CIF data deposited in the Cambridge Structural Database.

aryl groups ($\mathbf{L^3} > \mathbf{L^1} > \mathbf{L^2}$) causes an increased twist angle and decreased bite angle, which result in shorter Pd···Pd distances. The effect of substitution of the *meso*-CMe_2 groups with CPh_2 (i.e., $[Pd_2(\mathbf{L^4})]$, $[Pd_2(\mathbf{L^5})]$) is less clear, although this does result in an increased twist angle as a consequence of the more sterically demanding *endo*-phenyl substituents, and, for $[Pd_2(\mathbf{L^4})]$, increases the Pd···Pd separation.

The syntheses of related diiron complexes of **L**, $[Fe_2(\mu\text{-O})(\mathbf{L})]$, have been reported by Sessler and co-workers, who found that similar Pacman structural motifs were adopted in the solid state.[28] As with $[Pd_2(\mathbf{L})]$, the binuclear molecular-cleft structure is reinforced by the presence of the *o*-aryl hinge, although, in this case, the incorporation of the metal-bridging oxo group does not allow torsional twist (0.3°) and therefore promotes a close M···M separation (3.145 Å). Furthermore, we have also observed that monometallic uranyl complexes of **L**, for example, $[UO_2(thf)(H_2\mathbf{L^1})]$, adopt wedged structures in which the pyrrolic hydrogen atoms of the metal-free N_4-donor compartment form hydrogen bonds to the *endo*-uranyl oxygen atom; this results in significant lengthening of the *endo*-U=O compared to the *exo*-U=O moiety.[40] The importance of the *o*-aryl hinge in promoting the rigid Pacman structural motif is evident by comparison to similar binuclear accordion Schiff-base diporphyrin and calixpyrrole complexes that have been structurally characterised by Bowman-James and co-workers,[19,20] and Brooker and co-workers, respectively.[30] In both of these cases, the presence of conformationally labile alkyl-chain linkers between the two N_4 donor compartments results in flattened structures in which the metal atoms are highly separated (M···M 5.39–8.38 Å).

Nickel complexes: The reactions between hydrated $NiCl_2$ and $H_4\mathbf{L}$ ($\mathbf{L} = \mathbf{L^1}$ and $\mathbf{L^5}$) in the presence of Et_3N do not result in the expected binuclear complexes $[Ni_2(\mathbf{L})]$, but rather the methoxy- and hydroxy-bridged adducts $[Ni_2(\mu\text{-OMe})_2Cl_2(HOMe)_2(H_4\mathbf{L^1})]$, and $[Ni_2(\mu\text{-OH})_2Cl_2(HOMe)(H_4\mathbf{L^5})]$, respectively (Scheme 3). Elemental analytical data for these orange solids support the proposed molecular formulae, and the IR spectra of $[Ni_2(\mu\text{-OMe})_2Cl_2(HOMe)_2(H_4\mathbf{L^1})]$ and $[Ni_2(\mu\text{-OH})_2Cl_2(HOMe)(H_4\mathbf{L^5})]$ show bands at 1615 and 1617 cm^{-1}, respectively, characteristic of ν(C=N) stretching vibrations. The electrospray mass spectrum of $[Ni_2(\mu\text{-OMe})_2Cl_2(HOMe)_2(H_4\mathbf{L^1})]$ displays a parent ion at *m*/*z* 792 (100) with the correct isotopic pattern for $[Ni_2Cl_2(H_4\mathbf{L^1})]^+$, while $[Ni_2(\mu\text{-OH})_2Cl_2(HOMe)(H_4\mathbf{L^5})]$ shows a molecular ion peak at *m*/*z* 1024 assigned to the binuclear fragment $[Ni_2(H_4\mathbf{L^5})]^+$. The ^1H NMR spectra of both Ni^{II} complexes are featureless.

Structural characterisation of $[Ni_2(\mu\text{-OMe})_2Cl_2(HOMe)_2(H_4\mathbf{L^1})]$ and $[Ni_2(\mu\text{-OH})_2Cl_2(HOMe)(H_4\mathbf{L^5})]$: Orange plates suitable for X-ray crystallography were grown by slow diffusion of diethyl ether into $MeOH/CH_2Cl_2$ solutions, and the solid-state structures determined (Figure 4); selected bond lengths and angles are displayed in Table 4.

The X-ray crystal structure of $[Ni_2(\mu\text{-OMe})_2Cl_2(HOMe)_2(H_4L^1)]$ confirms that the Ni^{II} centres each adopt octahedral geometries in which the sum of the equatorial angles for Ni1 and Ni2 are 359.9 and 359.8°, respectively, and the axial Cl1-Ni1-O3 and O4-Ni2-Cl2 angles are 176.36(13) and 176.73(14)°. The Ni^{II} centres are bound to the imine nitrogen donors of the macrocycle only, whilst the other equatorial sites are occupied by two methoxy bridges that link the two metal centres; the axial positions of both cations are occupied by a chloride anion and a neutral MeOH molecule in a transoid configuration. It is presumed that the methoxy groups derive from the deprotonation of MeOH solvent under the basic reaction conditions. The Ni–N(imine) bond lengths range from 2.089(5) to 2.136(6) Å and are similar to those seen in the crystallographically characterised binuclear Ni^{II} complex that results from the $Ni(OAc)_2$-templated condensation between pyrrole-2,5-dicarbaldehyde and *o*-phenylenediamine.[41] No significant differences were observed between the bridging Ni–OMe bond lengths, which range from 2.053(4) to 2.080(4) Å and are shorter than the terminal Ni–MeOH distances (Ni1–O3 2.215(4) and Ni2–O4 2.233(4) Å). The Ni1–Cl1 and Ni2–Cl2 bond lengths (2.4660(16) and 2.4371(17) Å, respectively) are similar to those in the structurally related $[Ni(\mu\text{-Cl})_2(N,OH)_2]Cl_2$, (N,OH = 2-(4,4-dimethyl-4,5-dihydrooxazol-2-yl)-propan-2-ol).[42] The pyrrole nitrogen atoms remain protonated and form hydrogen bonds primarily to the methoxy ligands that bridge the Ni cations (O1···N2 2.856, O1···N3 3.007, O2···N6 2.919, O2···N7 2.906 Å), although close contacts between the pyrrole nitrogen atoms and axial chloro and MeOH ligands are also observed (N3···Cl2 3.127, N6···Cl2 3.147, N2···O3 3.152, N7···O3 3.012 Å).

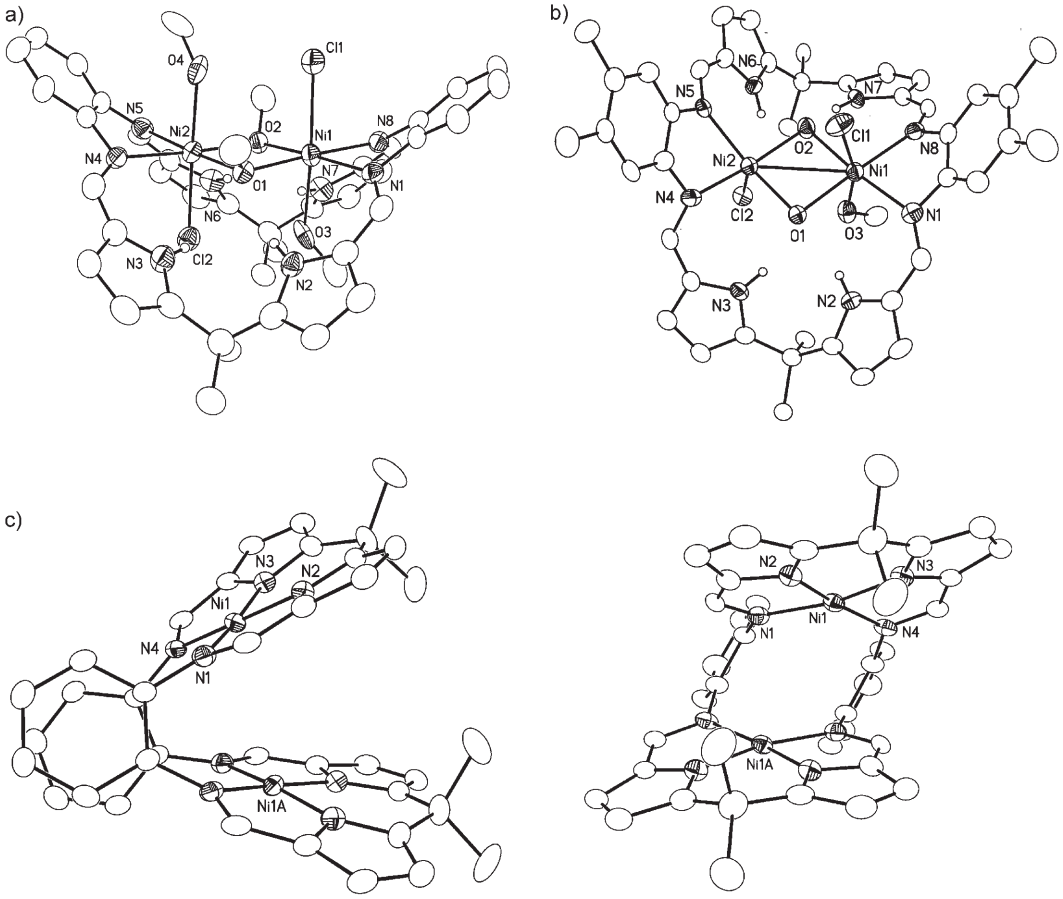

Figure 4. Solid-state structures of a) $[Ni_2(\mu\text{-}OMe)_2Cl_2(HOMe)_2(H_4\mathbf{L^1})]$, b) $[Ni_2(\mu\text{-}OH)_2Cl_2(HOMe)(H_4\mathbf{L^5})]$, and c) $[Ni_2(\mathbf{L^1})]$; displacement ellipsoids are drawn at 50% probability. For clarity, all hydrogen atoms, except those involved in hydrogen bonding in $[Ni_2(\mu\text{-}OMe)_2Cl_2(HOMe)_2(H_4\mathbf{L^1})]$ and $[Ni_2(\mu\text{-}OH)_2Cl_2(HOMe)(H_4\mathbf{L^5})]$, aryl carbon atoms except the *ipso*-C atoms in $[Ni_2(\mu\text{-}OH)_2Cl_2(HOMe)(H_4\mathbf{L^5})]$ and solvent molecules have been omitted.

The presence of the methoxy bridges results in a relatively short Ni···Ni separation of 3.122 Å, albeit longer than that reported for the above-mentioned binuclear Ni^{II} complex, in which constraints of the fully conjugated macrocycle plus extra acetate ligands result in a Ni···Ni separation of 2.512 Å. However, the Ni···Ni distance in $[Ni_2(\mu\text{-}OMe)_2Cl_2(HOMe)_2(H_4\mathbf{L^1})]$ can be considered short and comparable with those in related binuclear Ni^{II} Schiff-base complexes.[43]

The solid-state structure of $[Ni_2(\mu\text{-}OH)_2Cl_2(HOMe)(H_4\mathbf{L^5})]$ (Figure 4) is similar to that of $[Ni_2(\mu\text{-}OMe)_2Cl_2(HOMe)_2(H_4\mathbf{L^1})]$ in that the Ni cations are co-ordinated to the macrocycle through the imine nitrogen atoms only, and the pyrrole nitrogen atoms remain protonated. However, in $[Ni_2(\mu\text{-}OH)_2Cl_2(HOMe)(H_4\mathbf{L^5})]$, the dinickel core is linked by two hydroxy bridges, presumably resulting from deprotonation of water under the basic reaction conditions, and one Ni^{II} centre, Ni2, displays a square-pyramidal geometry. As with $[Ni_2(\mu\text{-}OMe)_2Cl_2(HOMe)_2(H_4\mathbf{L^1})]$, the equatorial chloro ligands in $[Ni_2(\mu\text{-}OH)_2Cl_2(HOMe)(H_4\mathbf{L^5})]$ adopt a transoid conformation, although Cl1 is tilted towards the vacant site on Ni2 (Ni2-Ni1-Cl1 80.29(5)°). Hydrogen-bonding interactions between the pyrrolic NH groups and the axial and equatorial ligands on the Ni^{II} cations are again evident (N2···O1 2.870, N3···O1 2.749, N6···Cl2 3.307, N6···O2 2.767 and N7···O2 2.717 Å). The Ni···Ni distance of 2.9660(11) Å is contracted compared to that of $[Ni_2(\mu\text{-}OMe)_2Cl_2(HOMe)_2(H_4\mathbf{L^1})]$ (3.122 Å), and is presumably a consequence of the relaxation of steric demand due to the presence of five-co-ordinate Ni2.

Dimetallic complexes of $H_4\mathbf{L}$ in which the ligand remains protonated have been observed previously by us in the d^{10} adducts $[Cd_2(OAc)_4(H_4\mathbf{L^1})]$ and $[Zn_2(H_4\mathbf{L^1})](BF_4)_2$.[44] As in $[Ni_2(\mu\text{-}OMe)_2Cl_2(HOMe)_2(H_4\mathbf{L^1})]$ and $[Ni_2(\mu\text{-}OH)_2Cl_2(HOMe)(H_4\mathbf{L^5})]$, only Cd–N(imine) binding was observed in $[Cd_2(OAc)_4(H_4\mathbf{L^1})]$, with the protonated pyrrolic centres participating in hydrogen-bonding interactions with acetate ligands, both in the solid state and in solution. Interestingly, Sessler and co-workers have synthesised the Cu^{II} complex $[(CuCl)_2(H_4\mathbf{L^1})]$, in which each metal centre is bound similarly to only the imine nitrogen atoms while the remaining protonated pyrrole groups are involved in intramolecular hydrogen-bonding interactions.[27] Thus, macrocycle **L** can accommodate metal salts in a variety of ways, and hinged conformations in the resultant binuclear complexes are preferred only when complete deprotonation of $H_4\mathbf{L}$ is achieved.

Table 4. Selected bond lengths [Å] and angles [°] for the dinickel complexes $[Ni_2(\mu\text{-}OMe)_2Cl_2(HOMe)_2(H_4\mathbf{L^1})]$ and $[Ni_2(\mu\text{-}OH)_2Cl_2(HOMe)(H_4\mathbf{L^5})]$.

	$[Ni_2(\mu\text{-}OMe)_2Cl_2(HOMe)_2(H_4\mathbf{L^1})]$	$[Ni_2(\mu\text{-}OH)_2Cl_2(HOMe)(H_4\mathbf{L^5})]$
Ni1–N1	2.136(6)	2.116(5)
Ni1–N8	2.131(4)	2.089(5)
Ni1–O1	2.053(4)	2.055(4)
Ni1–O2	2.080(5)	2.017(4)
Ni1–O3	2.215(4)	2.316(4)
Ni1–Cl1	2.4660(16)	2.4091(17)
Ni2–N4	2.153(5)	2.050(5)
Ni2–N5	2.141(6)	2.063(4)
Ni2–O1	2.061(5)	2.027(4)
Ni2–O2	2.057(4)	2.031(4)
Ni2–O4	2.233(4)	–
Ni2–Cl2	2.4371(17)	2.3256(18)
Ni···Ni	–	2.9660(11)
O1-Ni1-O2	81.32(16)	85.93(15)
N1-Ni1-N8	77.39(18)	77.73(18)
O1-Ni1-N1	100.96(17)	98.90(17)
O2-Ni1-N8	100.20(17)	97.35(16)
Cl1-Ni1-O3	176.36(13)	164.03(12)
Cl1-Ni1-Ni2	–	80.29(5)
O1-Ni2-O2	81.72(16)	86.31(15)
N4-Ni2-N5	78.41(18)	79.75(18)
O1-Ni2-N4	100.73(17)	93.11(16)
O2-Ni2-N5	98.96(17)	95.29(16)
Cl2-Ni2-O4	176.76(14)	–
Cl2-Ni1-Ni2	–	99.10(5)

Synthesis and structural characterisation of $[Ni_2(\mathbf{L^1})]$: Deprotonation of $H_4\mathbf{L^1}$ with KH in THF and subsequent reaction of the resulting potassium salt $K_4\mathbf{L^1}$ with $[NiCl_2(dme)]$ in boiling THF results in formation of the red, binuclear complex $[Ni_2(\mathbf{L^1})]$ in moderate yield; elemental analytical data support this formulation. The ^{1}H NMR spectrum of $[Ni_2(\mathbf{L^1})]$ shows a single resonance characteristic of the imine at $\delta = 6.64$ ppm, and the presence of two separate singlets for *endo*- and *exo-meso*-CH_3 groups at $\delta = 1.57$ and 1.35 ppm suggests that a wedged structure is adopted in solution. The single-crystal X-ray structure of $[Ni_2(\mathbf{L^1})]$ was determined for red blocks grown from cooled toluene/pentane (Figure 4); selected bond lengths and angles are detailed in Table 2. As expected from the above NMR data, the Ni^{II} centre adopts a distorted square-planar geometry within the N_4-donor pocket (sum of angles 360.2°) with average Ni–N(pyrrole) and Ni–N(imine) bond lengths of 1.821 and 1.930 Å, respectively. The Ni–N(imine) bond lengths are significantly shorter than those in $[Ni_2(\mu\text{-}OMe)_2Cl_2(HOMe)_2(H_4\mathbf{L^1})]$ and $[Ni_2(\mu\text{-}OH)_2Cl_2(HOMe)(H_4\mathbf{L^5})]$, and this is attributable to the reduced co-ordination number in $[Ni_2(\mathbf{L^1})]$; similar Ni–N(imine) bond lengths are seen in related dinickel Schiff-base complexes synthesised by Brooker and co-workers.[30] The Ni···Ni separation of 3.632 Å in $[Ni_2(\mathbf{L^1})]$ is considerably shorter than that of both the single-pillared Pacman analogue $[Ni_2(DPX)]$[45] (4.689 Å, Scheme 1) and the related dinickel accordion Schiff-base calixpyrrole (6.682 Å),[30] and reflects the decreased ionic radius of Ni^{II}. Furthermore, dinickel diporphyrins which incorporate a flexible calixarene separator display close interporphyrin contacts (3.30–3.40 Å).[46] The decrease in the Ni···Ni separation in $[Ni_2(\mathbf{L^1})]$ is also facilitated by its highly twisted conformation ($\Phi = 30.3°$), and reflects a decrease in steric repulsion between the *endo-meso*-substituents; a similarly large torsional angle (22.2°) is observed for $[Ni_2(DPX)]$.[45]

Copper complexes: The reactions between $H_4\mathbf{L}$ and $Cu(BF_4)_2{\cdot}H_2O$ in the presence of Et_3N afford the binuclear complexes $[Cu_2(\mathbf{L})]$ ($\mathbf{L} = \mathbf{L^1}$, $\mathbf{L^2}$, $\mathbf{L^3}$) as brown/purple solids in 43–87 % yields (see Scheme 3). While this work was in progress, Sessler and co-workers reported an alternative synthesis of $[Cu_2(\mathbf{L^1})]$ from the reaction of $H_4\mathbf{L^1}$ and Cu(mesityl) followed by aerial oxidation;[27] we shall concentrate this discussion on naphthylene-hinged complex $[Cu_2(\mathbf{L^3})]$. The IR spectrum of $[Cu_2(\mathbf{L^3})]$ shows an absorption at 1564 cm^{-1} that is characteristic of an imine/pyrrole ν(C=N) stretching vibration. The electrospray mass spectrum shows a molecular ion at m/z 827 and confirms the binuclear nature of $[Cu_2(\mathbf{L^3})]$; elemental analytic data also support this formulation. The paramagnetism of the Cu^{II} centres precludes the use of ^{1}H NMR spectroscopy to establish the co-ordination geometry of $[Cu_2(\mathbf{L^3})]$ in solution. However, the room-temperature solution magnetic moment was determined by Evans' method[47] to be 2.64 μ_B, a value which is intermediate between those expected for either two magnetically independent d^9 centres ($S = {}^1/_2 + {}^1/_2$, 2.45 μ_B) or for a binuclear triplet ($S = 1$, 2.83 μ_B), and is indicative of some degree of antiferromagnetic coupling (see EPR discussion below). Sessler and co-workers investigated the magnetic properties of $[Cu_2(\mathbf{L^1})]$ in solution at 300 K ($\mu_{eff} = 2.00$ μ_B), and also in the solid state between 4 and 300 K, and observed a weak antiferromagnetic interaction between the two Cu centres; simulation of these solid-state data with a modified Bleaney–Bowers equation resulted in a fit with a J value of (-41 ± 0.2) cm^{-1}.[27]

Crystallographic characterisation of $[Cu_2(\mathbf{L^3})]$ and $[Cu_2(\mu\text{-}py)(\mathbf{L^3})]$: Purple needles of $[Cu_2(\mathbf{L^3})]$ were grown from a saturated solution in $CHCl_3$ and the X-ray crystal structure determined; the crystal structures of $[Cu_2(\mathbf{L^1})]$ and $[Cu_2(\mathbf{L^2})]$ were also determined for comparison, and are described in the Supporting Information. The solid-state structure of $[Cu_2(\mathbf{L^3})]$ is shown in Figure 5, and selected bond lengths and angles are displayed in Table 2.

As in $[Ni_2(\mathbf{L^1})]$, the dicopper complexes $[Cu_2(\mathbf{L})]$ adopt wedged structural motifs in which the macrocyclic framework is distorted, presumably as a consequence of the decreased ionic radius of Cu^{II}. In $[Cu_2(\mathbf{L^3})]$, the Cu centres are square-planar (sum of angles at Cu1 359.88°, 0.068 Å o.o.p.; sum of angles at Cu2 359.71°, 0.065 Å o.o.p.), with average Cu–N(pyrrole) and Cu–N(imine) bond lengths of 1.909 and 2.029 Å, respectively. As with $[Pd_2(\mathbf{L^3})]$, the presence of naphthylene hinges appears to induce increased torsional twist which results in a relatively short Cu···Cu separation (3.552 Å). Significantly, however, Sessler and co-workers have recently reported two X-ray crystal structure determinations of $[Cu_2(\mathbf{L^1})]$,[27] in which the Cu···Cu separations are

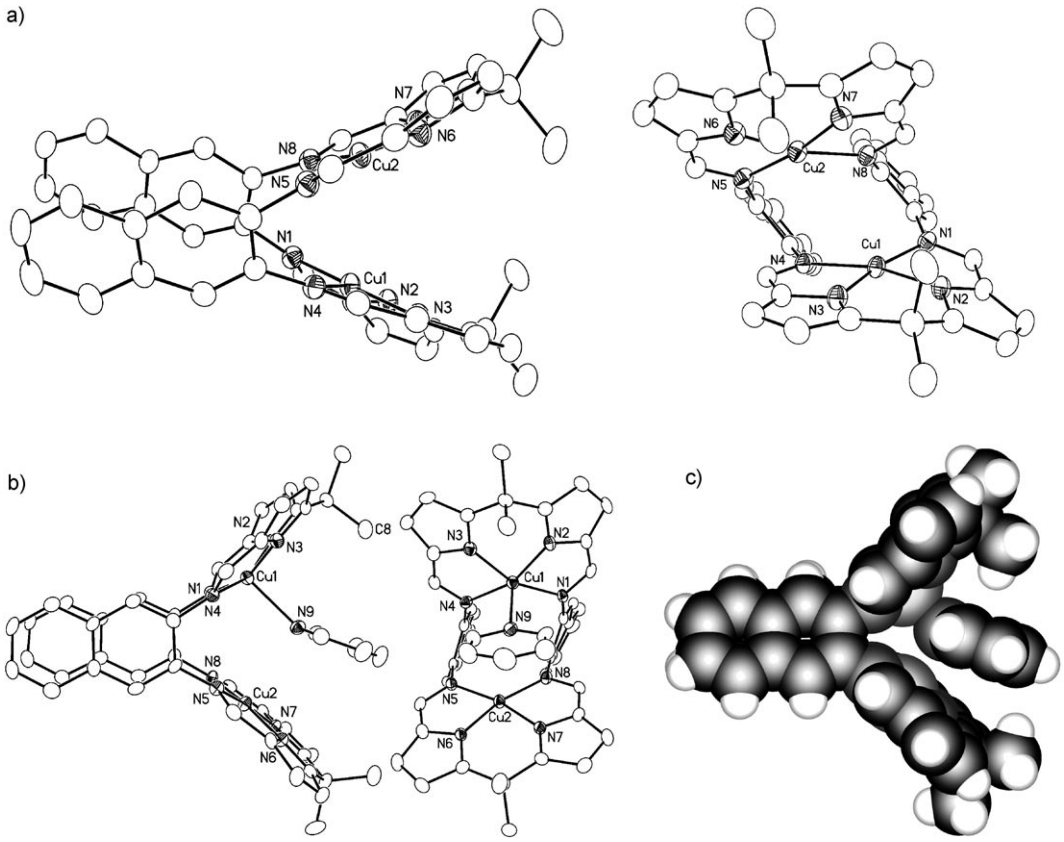

Figure 5. Solid-state structures of a) $[Cu_2(\mathbf{L^3})]$, b) $[Cu_2(\mu\text{-py})(\mathbf{L^3})]$ and c) a space-filling drawing of $[Cu_2(\mu\text{-py})(\mathbf{L^3})]$. For clarity, all hydrogen atoms and solvent molecules have been omitted; displacement ellipsoids are drawn at 50% probability.

3.473 and 4.053 Å, respectively; these values are different to the Cu···Cu separation of 4.014 Å from our structural determination of $[Cu_2(\mathbf{L^1})]$. It therefore appears that the intermetallic distances in this series of dicopper complexes are unpredictable, and differences may, in part, be due to crystal packing effects. Even so, the variation of intermetallic distance remains small (ca. 0.5–0.6 Å), which reinforces further the perception that this general class of complexes is unable to undergo vertical expansion to the same degree as the Pacman diporphyrinic analogues, and so results in a highly spatially confined binuclear molecular cleft.

A consequence of this constrained geometry is exemplified by formation of the mono-pyridine adduct $[Cu_2(\mu\text{-py})(\mathbf{L^3})]$, which results from crystallisation of $[Cu_2(\mathbf{L^3})]$ in the presence of an excess of pyridine; the elemental analytical data for $[Cu_2(\mu\text{-py})(\mathbf{L^3})]$ support the presence of a single pyridine molecule. The single-crystal X-ray structure of $[Cu_2(\mu\text{-py})(\mathbf{L^3})]$ is shown in Figure 5, with selected bond lengths and angles detailed in Table 2. Interestingly, the structure reveals that the two Cu centres in $[Cu_2(\mu\text{-py})(\mathbf{L^3})]$ are inequivalent with the pyridine bound within the cleft of the calixpyrrole metallohost. Cu1 adopts a square-pyramidal geometry in which the metal centre sits 0.343 Å above the basal plane and N9 of pyridine occupies the apical position (Cu1–N9 2.258(3) Å), while Cu2 remains square-planar (sum of angles at Cu2 359.68°) bound within the N_4-donor plane (0.060 Å o.o.p), and has little or no interaction with the pyridine N donor (Cu2···N9 2.983 Å). To accommodate the pyridine ligand within the cleft, the hinge angle between the CuN_4 planes expands from 53.3° in $[Cu_2(\mathbf{L^3})]$ to 59.9° in $[Cu_2(\mu\text{-py})(\mathbf{L^3})]$, and the macrocycle undergoes a 12.6° reduction in torsional twist; this results in an increase of the Cu1···Cu2 separation to 4.014 Å. Furthermore, to fit within the cleft, the pyridine molecule adopts an unusual canted geometry in which the Cu1–N9 bond does not lie in the plane of the C_5H_5N ring, and this results in a Cu1-N9-(pyridine centroid) angle of 155.2°. This canted geometry also appears to be reinforced by a hydrogen-bonding interaction between the C8 *meso*-methyl proton and the pyridine ring (C8···centroid 3.686 Å; Figure 5c). The bonding of pyridine within the dicopper cleft of $[Cu_2(\mu\text{-py})(\mathbf{L^3})]$ is best described as a combination of Cu–N co-ordination and a host–guest interaction, and reflects the high rigidity of the binuclear cleft environment. In contrast, binuclear copper helicates of terpyridine or (bis-imino)pyridine ligands display structures in which the pyridyl N atoms bridge the two metal centres, with Cu–N(pyridine) distances that range from 2.180 to 2.712 Å; furthermore, these bridging pyridyl groups are twisted with respect to the Cu···Cu vector due to the overall helicity of these dicopper systems.[48]

Bimetallic cofacial diporphyrins have been found previously to act as hosts for guest molecules, in particular for

guests incorporating two donor atoms that encourage bimetallic binding. For example, the dizinc complex [Zn_2(DPD)], where DPD is a diporphyrin ligand with a dibenzofuran spacer, acts as a 1:1 host for 2-aminopyrimidine, which is bound to both Zn ions within the diporphyrinic cavity.[49] This actually results in the vertical closure of the molecule, with a Zn···Zn separation of 6.684 Å compared to 7.775 Å in the free host, although both of these M···M separations are considerably longer than that in [Cu_2(μ-py)(**L**^{3})]. Molecules such as 1,4-diazabicyclo[2.2.2]octane (DABCO) and even C_{60} have been bound within Pacman clefts by using strategies that elongate the spacer between the two porphyrin units. For example, calixarene or diarylurea spacers provide a rigid, yet sufficiently elongated separation between Zn(porphyrin) units to accommodate DABCO,[50] while the use of a *trans*-substituted $PdCl_2$(pyridylporphyrin)$_2$ complex as spacer results in a cavity large enough to host C_{60}.[51]

EPR spectroscopy of [Cu_2(L**^{1})], [Cu_2(**L**^{3})] and [Cu_2(μ-py)(**L**^{3})]**: The EPR spectra of the binuclear complexes [Cu_2(**L**^{1})] and [Cu_2(**L**^{3})] have been examined for a combination of X (9.7 GHz), Q (35 GHz) and S (3 GHz) bands in frozen 2-methyltetrahydrofuran (Me-THF) glass, and the X-band spectra are shown in Figure 6.

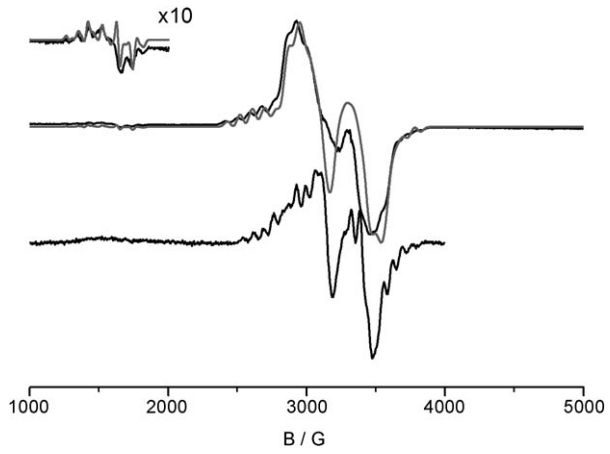

Figure 6. X-band EPR spectra of the dicopper complexes [Cu_2(**L**^{1})] (top; inset: $\Delta M_S = \pm 2$ signal) and [Cu_2(**L**^{3})] (bottom). Experimental spectra (black) and simulation for [Cu_2(**L**^{1})] (grey) with the parameters in the text.

The spectra are typical of an $S=1$ spin triplet, as evidenced by both the zero-field splitting of the $\Delta M_S = 1$ lines and the appearance of a "forbidden" $\Delta M_S = 2$ "half-field" transition,[52] with resolution of nuclear hyperfine coupling to two ^{63,65}Cu nuclei, but not to the co-ordinated ^{14}N nucleus. Such spectra can, in principle, be analysed to give information on the separation and relative orientations of the paramagnetic ions. Thus, the X-band EPR spectrum of [Cu_2(**L**^{1})] was simulated by using a full-interaction spin Hamiltonian incorporating the g and ^{63,65}Cu nuclear hyperfine (A) matrices of the individual Cu^{II} ions, and a magnetic exchange matrix (J) containing isotropic and anisotropic components, the latter being determined by the Cu···Cu distance (r) in a dipolar approximation [Eq. (1)], where β is the electronic Bohr magneton, and B the applied magnetic field.

$$\hat{H} = \sum_{i=1,2} (\beta B g \hat{S}_i + \hat{S}_i A \hat{I}_i) + \hat{S}_1 \cdot J \cdot \hat{S}_2 \qquad (1)$$

This allows determination of r and of the relative orientations of the co-ordination planes of the Cu centres to the Cu···Cu vector. However, because the co-ordination planes of the two Cu centres are not co-planar in [Cu_2(**L**^{1})], we must also consider the relative orientations of the two Cu centres to each other as well as to the Cu···Cu vector. This contrasts with the approach of Eaton and co-workers for co-facial dicopper diporphyrins[53] in which the CuN_4 compartments are coplanar and where the local reference frames of the two Cu ions are coincident; this significantly reduces the number of parameters required compared to those for [Cu_2(**L**^{1})].[54] The procedures used to determine the spin Hamiltonian and structural parameters are detailed in the Supporting Information.

We initially assumed the solution structure of [Cu_2(**L**^{1})] to be that found in the solid state and this afforded the relative orientations of the g, A and J matrices. In this assumption the two-fold symmetry requires the two Cu centres to have identical parameters, and we further assumed axial local symmetry at each Cu centre. We refined the simulations, including the relative orientations, from this starting point. Good simulations were obtained with $g_{xx}=g_{yy}=2.02$, $g_{zz}=2.16$, $A_{xx}=A_{yy}=20\times10^{-4}$ cm^{-1}, $A_{zz}=210\times10^{-4}$ cm^{-1} for both Cu centres, typical of square-planar {CuN_4} species, with an interspin distance of $r=(4.1\pm0.05)$ Å and an angle between the $g_{zz}(A_{zz})$ axes of the two Cu ions of $\theta=(60\pm2)°$. The analysis gave an angle between the local $g_{zz}(A_{zz})$ axes and the Cu···Cu vector of $\rho=(43\pm2)°$, and an arbitrarily high isotropic exchange constant of 20 cm^{-1} ($\gg g\beta B_{res} > A/g\beta$, that is, there is no singlet–triplet mixing). Note that the large angle $\rho\approx45°$ leads to almost equal observed Cu hyperfine splittings in the "parallel" and "perpendicular" parts of the EPR spectrum.

The optimised structural parameters obtained from the frozen-solution EPR spectra do not vary significantly from the initial values taken from the single-crystal X-ray structure ($\theta=60°$, $\rho=43°$, $r=4.014$ Å), that is, the initial assumption of very similar solution and solid-state structures appears to be valid. A further measure of the Cu···Cu separation can be obtained from the relative intensities of the $\Delta M_S=2$ to $\Delta M_S=1$ transitions,[53] provided that the metal–metal separation is long enough for the point-dipole approximation to be valid.[55] Evaluating the double integral of these two regions of the X-band spectrum of [Cu_2(**L**^{1})] and using Eaton's equation[53] gives $r=3.8$ Å, again relatively close to that observed in the single-crystal X-ray structure.

Although the spectra of [Cu_2(**L**^{3})] are qualitatively similar to those of [Cu_2(**L**^{1})] (Figure 6), there are two important differences. Firstly, the spread in magnetic field of the allowed signals is slightly smaller in [Cu_2(**L**^{3})] compared to

$[Cu_2(\mathbf{L^1})]$. Secondly, the relative intensity of the half-field signal is lower for $[Cu_2(\mathbf{L^3})]$. Both these factors imply that the dipolar coupling is slightly weaker in $[Cu_2(\mathbf{L^3})]$ and that, therefore, in solution the Cu···Cu separation is slightly greater. Quantifying this separation from the relative intensity of the half-field transition at X-band is problematical due to weak signal intensity and relatively low resolution. Although the relative intensity of this feature can be enhanced by measuring at lower frequency (e.g., S-band, see Supporting Information), this also leads to overlapping of the two regions of the spectrum. A slightly larger Cu···Cu separation for $[Cu_2(\mathbf{L^3})]$ contradicts the single-crystal X-ray diffraction data, which give Cu···Cu separations of 4.01 and 3.55 Å for $[Cu_2(\mathbf{L^1})]$ and $[Cu_2(\mathbf{L^3})]$, respectively. This implies that the structure of $[Cu_2(\mathbf{L^3})]$ relaxes significantly in solution, to resemble that of $[Cu_2(\mathbf{L^1})]$, in keeping with the fact that the bite angle (and hence Cu···Cu separation) of $[Cu_2(\mathbf{L^3})]$ can increase to accommodate guest molecules such as pyridine (see above).

The insertion of a molecule of pyridine within the cleft, as in $[Cu_2(\mu\text{-py})(\mathbf{L^3})]$, while producing a significant effect in the solid-state structure, does not appear to affect the EPR spectrum of $[Cu_2(\mu\text{-py})(\mathbf{L^3})]$ in frozen solution. The EPR spectra of crystalline $[Cu_2(\mu\text{-py})(\mathbf{L^3})]$ dissolved in Me-THF, and $[Cu_2(\mathbf{L^3})]$ dissolved in an excess of pyridine are very similar, and show little difference to the parent, pyridine-free complex $[Cu_2(\mathbf{L^3})]$. It is, therefore, likely that co-ordination of pyridine in $[Cu_2(\mu\text{-py})(\mathbf{L^3})]$ is a solid-state effect, probably due to favourable crystal packing energies, that is lost when the sample is dissolved. Unfortunately, solid-state powder spectra of $[Cu_2(\mathbf{L^3})]$ and $[Cu_2(\mu\text{-py})(\mathbf{L^3})]$ are very broad and no meaningful conclusions could be reached.

It is, therefore, clear that the inability of $[M_2(\mathbf{L})]$ complexes to undergo appreciable vertical cleft expansion mitigates against the co-ordination of donor solvents within the binuclear cleft. This is in contrast to binuclear cofacial diporphyrins, which can accommodate solvents such as pyridine in more normal co-ordination modes within the cleft; usually, bulky N-donor ligands such as *tert*-butylimidazole are employed as axial base to ensure that no *endo* co-ordination occurs. The *endo* o-ordination of small N-donor ligands by single-pillared diporphyrin complexes is exemplified by the X-ray crystal structures of the dicobalt bis-corrole and the porphyrin-corrole complexes [Co(*exo*-py)Co(*endo*-py)(*exo*-py)(BCA)] and [Co(*exo*-py)(*endo*-py)(H_2PCX)], respectively, where BCA is an anthracyl-bridged bis-corrole ligand and (H_2PCX) is a xanthyl-bridged porphyrin-corrole ligand in which the porphyrin cavity is unoccupied.[16,56] In both of these cases, one cobalt centre is octahedral with one of the axial pyridine ligands bound within the binuclear cleft; even so, and unlike $[Cu_2(\mu\text{-py})(\mathbf{L^3})]$, the wide-ranging vertical expansion available to these ligand systems still results in nearly linear N(py)-Co-N(py) angles.

Synthesis and structural characterisation of the manganese complex $[Mn_2(\mathbf{L^1})]$: Attempts to synthesise a binuclear manganese complex of $H_4\mathbf{L^1}$ by using simple Mn^{II} salts such as $Mn(OAc)_2$ or $MnCl_2$ in the presence of Et_3N were unsuccessful. However, the transamination reaction between $H_4\mathbf{L^1}$ and the Mn^{II} amide $[Mn(thf)_2\{N(SiMe_3)_2\}_2]$ results in formation of the very air sensitive $[Mn_2(\mathbf{L^1})]$ as a red powder; this formulation is supported by elemental analysis. X-ray-quality crystals were grown from hot toluene, and the structure determined (Figure 7); selected bond lengths and angles are

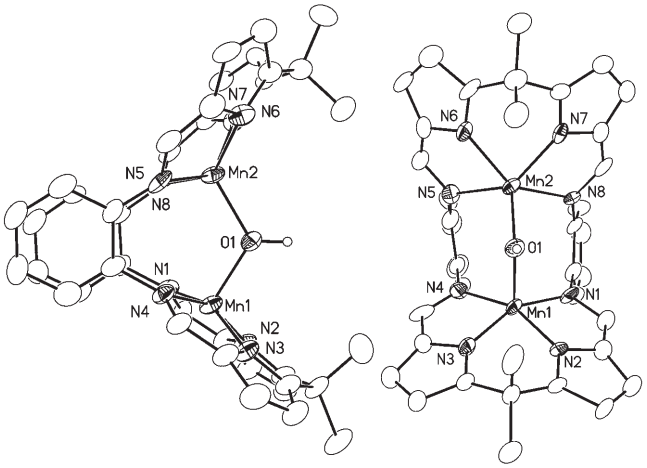

Figure 7. Solid-state structure of the dimanganese compound $[Mn_2(\mu\text{-OH})(\mathbf{L^1})]$ with displacement ellipsoids drawn at the 50% probability level. For clarity, all hydrogen atoms except that of the bridging OH ligand have been omitted.

detailed in Table 5. However, it is immediately clear that, upon crystallisation, reaction between $[Mn_2(\mathbf{L^1})]$ and traces of oxygen or water has occurred to form $[Mn_2(\mu\text{-OH})(\mathbf{L^1})]$,

Table 5. Selected bond lengths [Å] and angles [°] for $[Mn_2(\mu\text{-OH})(\mathbf{L^1})]$.

Mn1–N1	2.034(8)	N1-Mn1-N2	81.4(3)
Mn1–N2	1.917(7)	N2-Mn1-N3	83.2(3)
Mn1–N3	1.913(8)	N3-Mn1-N4	81.8(3)
Mn1–N4	2.041(7)	N4-Mn1-N1	104.9(3)
Mn1–O1	1.986(6)	N5-Mn2-N6	76.5(3)
Mn2–N5	2.211(8)	N6-Mn2-N7	79.1(3)
Mn2–N6	2.115(8)	N7-Mn2-N8	75.5(3)
Mn2–N7	2.079(8)	N8-Mn2-N5	103.9(3)
Mn2–N8	2.304(8)	Mn1-O1-Mn2	117.5(3)
Mn2–O1	2.011(6)		

in which a hydroxo ligand bridges the two Mn centres. The relatively low solution magnetic moment of 6.97 μ_B, as determined by Evans' method ($\mu_{calcd} = 8.37\ \mu_B$ for $Mn^{II}Mn^{II}$ non-interacting spins), suggests that oxidation of $[Mn_2(\mathbf{L^1})]$ in solution is facile. Furthermore, reactions between dry oxygen and binuclear Mn^{II} helicates have been observed to form, after H abstraction from the THF solvent, $Mn_2(\mu\text{-OH})$ and $Mn_2(\mu\text{-O})(\mu\text{-OH})$ bridging hydroxo complexes.[57]

The Mn–O1 bond lengths in $[Mn_2(\mu\text{-OH})(\mathbf{L^1})]$ are inequivalent (1.986(6) and 2.011(6) Å) with an Mn1-O1-Mn2 angle of 117.5(3)°. The Mn–O bond lengths in $[Mn_2(\mu\text{-OH})(\mathbf{L^1})]$ are comparable to those of other hydroxo-bridged dimanga-

nese porphyrins such as the Mn^{III}_2 dimer $[\{Mn(OEP)\}_2(\mu\text{-}OH)]^+$, which displays an Mn–O distance of 2.026(1) Å. However, the Mn-O-Mn angle in $[Mn_2(\mu\text{-}OH)(\mathbf{L^1})]$ is more acute than that of 152.73(11)° in the porphyrin system, but similar to those in complexes incorporating ancillary bridging ligands, for example, in $[\{(Tp)Mn\}_2(\mu^2{:}\kappa^1{:}\kappa^1\text{-pyrazolate})(\mu\text{-}OH)]$ (Tp = tris(pyrazolyl)borate, Mn-O-Mn 121.9(3)°). Both Mn centres in $[Mn_2(\mu\text{-}OH)(\mathbf{L^1})]$ adopt square-pyramidal geometries, but with significantly different metric parameters. For Mn1, the average Mn–N(pyrrole) and Mn–N(imine) bond lengths are 1.915 and 2.038 Å, while those associated with Mn2 are significantly longer (2.097 and 2.258 Å, respectively). Furthermore, Mn2 is significantly further out of the N_4 basal plane (0.71 Å) than Mn1 (0.38 Å) and, as described above, has a longer bond to O1. Thus, $[Mn_2(\mu\text{-}OH)(\mathbf{L^1})]$ is best described as a valence-localised $Mn^{II}Mn^{III}$ complex, in which the larger Mn^{II} cation is associated with the longer Mn2–N bond lengths.[58]

Significantly, dimanganese Pacman complexes in which the porphyrinic compartments are separated by an *o*-phenylene spacer have been shown by Naruta and co-workers to catalyse the oxidation of water to oxygen.[36,37] Some mechanistic details of this transformation have been elucidated by using a range of spectroscopic techniques, and it is thought that intermediate MnOH complexes are formed initially, which are further oxidised to Mn=O species prior to oxygen evolution. The implication of binuclear Mn hydroxides in this important process suggests that $[Mn_2(\mu\text{-}OH)(\mathbf{L^1})]$ may be a suitable structural model for oxygen-evolving dimanganese complexes.

Conclusion

We have described the synthesis of a series of metal complexes supported by the Schiff-base calixpyrroles $H_4\mathbf{L}$. The co-ordination mode of the macrocycle to the metal centres has been elucidated by X-ray crystallography, as well as by ^{1}H NMR and EPR spectroscopy where applicable. In particular, X-ray structural and spectroscopic analysis has shown that the majority of these binuclear complexes adopt structural motifs similar to those of single-pillared Pacman diporphyrins, and represent a straightforward and high-yielding approach to this important binuclear motif. Alternatively, synthetic procedures in which the pyrrolic nitrogen atoms of $H_4\mathbf{L}$ remain protonated promote the formation of binuclear adducts in which the metal centres are bound solely to the imine nitrogen atoms. Unlike their porphyrinic analogues, complexes of **L** appear to adopt significantly more rigid structures, as evidenced by the restricted vertical expansion and M···M separations in $[M_2(\mathbf{L})]$ complexes, and this feature may have important consequences in the reactivity of these systems. We are presently exploring the activity of bimetallic complexes of **L** as catalysts for the transformation of small molecules.

Experimental Section

General: The compounds $Me_2C(C_4H_2N\text{-}5,5'\text{-}CHO)_2$ (**i**),[25] $Ph_2C(C_4H_2N\text{-}5,5'\text{-}CHO)_2$ (**ii**)[22] and $[Mn(thf)_2\{N(SiMe_3)_2\}_2]$,[59] were synthesised according to literature procedures; all other reagents were used as purchased. THF and toluene were dried over activated alumina.[60] The ^{1}H and $^{13}C\{^1H\}$ NMR spectra were recorded on a Bruker DPX-300 spectrometer operating at 300.13 and 75.47 MHz, respectively; residual protio-solvent served as an internal reference for the former. Magnetic moments were determined in solution using Evans' method.[47] Elemental analyses were carried out by Mr. Stephen Boyer at the London Metropolitan University. Electrospray mass spectra were recorded using a Micromass LCT spectrometer, IR spectra on a Nicolet 210 FT-IR instrument and UV/Vis spectra on a Perkin-Elmer Lambda 5 UV/Vis spectrophotometer. EPR spectra were recorded on Bruker ESP (S- and Q-band) or Bruker EMX (X-band) spectrometers. Spectral simulations were performed using Bruker's XSophe software package. The crystal data for the structures determined in this work are given in Table 6.

Synthesis of tetratosylic acid salts: An equimolar mixture of dialdehyde **i** or **ii** and diamine in warm (ca. 40 °C) methanol was treated in portions with solid $TsOH\cdot H_2O$ (4 molar equiv). The resultant bright orange solution was stirred at 25 °C for 1 h, after which any precipitate was redissolved by warming. The mixture was allowed to stand at room temperature for 16 h, causing the deposition of the product as orange microcrystals which were collected on a glass frit and air-dried.

$H_4L^1(TsOH)_4$: Dialdehyde **i** (1.00 g, 4.33 mmol), 1,2-diaminobenzene (0.47 g, 4.33 mmol) and $HOTs\cdot H_2O$ (3.29 g, 0.017 mol) were combined; yield 72%. ^{1}H NMR ([D$_4$]methanol): δ_H = 8.53 (s, 4H, imine), 7.63 (m, 4H, H aryl), 7.47 (m, 8H, H aryl + pyrrole), 7.32 (AB d, 8H, arylsulfonyl), 7.01 (AB d, 8H, arylsulfonyl), 6.63 (d, 4H, $J_{H,H}$ = 4.3 Hz, pyrrole), 2.30 (s, 12H, Me arylsulfonyl), 1.94 ppm (s, 12H, Me); $^{13}C\{^1H\}$ NMR ([D$_6$]DMSO): δ_C = 159.6 (s, imine), 149.4 (s, quaternary), 142.7 (s, CH), 142.2 (s, CH), 136.3 (s, quaternary), 131.8 (s, quaternary), 130.7 (s, CH), 130.0 (s, CH), 126.7 (s, CH), 125.9 (s, quaternary), 121.5 (s, quaternary), 115.4 (s, CH), 26.0 (s, quaternary), 21.3 ppm (s, CH_3); IR (KBr): $\tilde{\nu}$3450, 3216, 2975, 1672, 1653, 1596, 1555, 1284 cm^{-1}. ES-MS: *m*/*z* (%): 777 [M^+ −3TsOH] (100); elemental analysis calcd (%) for $C_{66}H_{68}N_8O_{12}S_4$: C 61.29, H 5.30, N 8.66; found: C 61.24, H 5.45, N 8.51.

$H_4L^2(TsOH)_4$: Dialdehyde **i** (0.40 g, 1.73 mmol), 4,5-dimethyl-1,2-diaminobenzene (0.24 g, 1.73 mmol) and $HOTs\cdot H_2O$ (1.32 g, 6.93 mmol) were combined; yield 49%. ^{1}H NMR ([D$_4$]methanol): δ_H = 8.47 (s, 4H, imine), 7.36–7.30 (m, 16H, aryl + arylsulfonyl + pyrrole), 6.99 (AB d, 8H, arylsulfonyl), 6.57 (d, 4H, $J_{H,H}$ = 4.3 Hz, pyrrole), 2.31 (s, 12H, Me arylsulfonyl), 2.27 (s, 12H, Me), 1.93 ppm (s 12H, Me); this complex proved too insoluble for a $^{13}C\{^1H\}$ NMR spectrum to be recorded; ES-MS: *m*/*z* 833 [M^+ −3TsOH]; elemental analysis calcd (%) for $C_{70}H_{76}N_8O_{12}S_4$: C 62.29, H 5.67, N 8.30; found: C 62.19, H 5.57, N 8.14.

$H_4L^3(TsOH)_4$: Dialdehyde **i** (0.292 g, 1.27 mmol), 2,3-diaminonaphthalene (0.21 g, 1.33 mmol) and $HOTs\cdot H_2O$ (0.521 g, 2.74 mmol) were combined; yield 73%. ^{1}H NMR ([D$_4$]methanol): δ_H = 8.68 (s, 4H, imine), 7.98 (m, 4H, aryl), 7.87 (m, 4H, aryl), 7.54 (m, 8H, aryl + pyrrole), 7.41 (AB d, 8H, arylsulfonyl), 6.95 (AB d, 8H, arylsulfonyl), 6.64 (d, 4H, $J_{H,H}$ = 4.3 Hz, pyrrole), 2.17 (s, 12H, Me arylsulfonyl), 1.98 ppm (s, 12H, Me); this complex proved too insoluble for a $^{13}C\{^1H\}$ NMR spectrum to be recorded; IR (KBr): $\tilde{\nu}$3450, 3214, 3037, 2978, 1658, 1624, 1598, 1531, 1496, 1458, 1399, 1346, 1283, 1217, 1161, 1122, 1061, 1034, 1010 cm^{-1}; ES-MS: *m*/*z* (%): 877 [M^+−TsO] (100); elemental analysis calcd (%) for $C_{74}H_{72}N_8O_{12}S_4$: C 63.77, H 5.21, N 8.04; found: C 63.84, H 5.07, N 8.06.

$H_4L^4(TsOH)_4$: Dialdehyde **ii** (0.391 g, 1.10 mmol), 1,2-diaminobenzene (0.119 g, 1.10 mmol) and $HOTs\cdot H_2O$ (0.840 g, 4.42 mmol) were combined; yield 44%. ^{1}H NMR ([D$_4$]methanol): δ_H = 8.61 (br s, 4H, imine), 7.54 (AB d, 8H aryl sulfonyl), 7,48 (s, H, aryl phenyl), 7.35 (m, aryl phenyl), 7.24 (s, H aryl phenyl), 7.12 (AB d, 8H aryl sulfonyl), 2.30 ppm (s, 12H, CH_3); this complex proved too insoluble for a $^{13}C\{^1H\}$ NMR spectrum to be recorded; ES-MS: *m*/*z* (%): 853 [M^+−3TsOH] (100%); elemental analysis calcd (%) for $C_{86}H_{76}N_8O_{12}S_4$: C 66.99, H 4,97, N 7.27; found: C 66.72, H 4.73, N 6.98.

Table 6. Crystal data.[a]

	$H_4L^3(EtOH)_2$	$H_4L^6(H_2O)$	$[Pd_2(L^3)]$	$[Ni_2(\mu\text{-}OMe)_2Cl_2(HOMe)_2(H_4L^1)]$	$[Ni_2(\mu\text{-}OH)_2Cl_2(HOMe)(H_4L^5)]$
crystal size [mm]	0.64×0.26×0.21	0.60×0.07×0.06	0.31×0.16×0.04	0.22×0.14×0.11	0.44×0.12×0.10
crystal system	monoclinic	monoclinic	triclinic	orthorhombic	monoclinic
space group	$P2_1/c$	$C2/c$	$P\bar{1}$	$Pna2_1$	$C2/c$
a [Å]	12.9674(8)	13.747(2)	9.5614(6)	20.222(3)	29.876(5)
b [Å]	23.234(2)	27.268(3)	13.1871(9)	9.7982(15)	28.398(5)
c [Å]	15.1913(10)	14.872(2)	15.6343(10)	20.330(3)	15.491(3)
α [°]	90.00	90.00	101.425(1)	90.00	90.00
β [°]	101.976(2)	115.742(2)	92.199(1)	90.00	116.619(4)
γ [°]	90.00	90.00	100.410(1)	90.00	90.00
V [Å^3]	4477.3 (6)	5021.6 (11)	1894.8 (4)	4028.2 (10)	11750 (4)
Z, ρ_{exptl} [Mg m^{-3}]	4, 1.182	4, 1.127	2, 1.601	4, 1.516	8, 1.348
$2\theta_{max}$ [°]	51.0	44.4	55.0	54.4	43.0
measured, independent reflns	27266, 10237	15763, 5725	16324, 8564	24746, 9255	20891, 11276
reflns used in refinement	10237	5725	8561	8595	11276
absorption correction, T_{min}, T_{max}	none	none	0.819, 0.962	0.585, 0.643	0.691, 0.884
θ_{max} [°]	27.5	27.5	27.5	28.9	27.6
parameters	545	280	505	524	719
H-atom treatment	riding model, OH as rigid rotor	constrained, H_2O refined with restraints	constrained to parent site	constrained to parent site	constrained to parent site
$R[F^2>2\sigma(F^2)]$, $wR(F^2)$	0.044, 0.089	0.067, 0.157	0.031, 0.067	0.055, 0.148	0.076, 0.186
$\Delta\rho_{max}$, $\Delta\rho_{min}$ [e Å^{-3}]	0.20, −0.17	0.27, −0.20	0.50, −0.37	0.84, −0.54	0.93, −0.51
CSD numbers[b]	632813	632814	632815	632816	632817

	$[Ni_2(L^1)]$	$[Cu_2(L^3)]$	$[Cu_2(\mu\text{-py})(L^3)]$	$[Mn_2(\mu\text{-OH})(L^3)]$
crystal size [mm]	0.22×0.12×0.05	1.50×0.42×0.06	0.22×0.08×0.08	0.51×0.10×0.04
crystal system	orthorhombic	orthorhombic	triclinic	triclinic
space group	*Fddd*	*Pbca*	$P\bar{1}$	$P\bar{1}$
a [Å]	13.7359(15)	13.2534(13)	9.131(4)	15.965(3)
b [Å]	30.498(3)	24.807(3)	11.942(5)	18.173(4)
c [Å]	36.387(4)	26.755(3)	19.089(8)	18.723(4)
α [°]	90.00	90.00	93.448(7)	69.018(4)
β [°]	90.00	90.00	99.244(7)	81.972(4)
γ [°]	90.00	90.00	93.444(7)	78.815(3)
V [Å^3]	15243(5)	8796.4(17)	2046(2)	4961(3)
Z, ρ_{exptl} [Mg m^{-3}]	16, 1.316	8, 1.507	2, 1.473	4, 1.344
$2\theta_{max}$ [°]	49.8	55.0	48.4	36.8
measured, independent reflns	23789, 4726	54700, 11102	15135, 7206	35121, 17239
reflns used in refinement	4387	10108	7206	17238
absorption correction, T_{min}, T_{max}	multiscan, 0.712, 0.768	Multi-scan, 0.464, 1.000	multiscan, 0.695, 0.827	multiscan, 0.589, 1.000
θ_{max} [°]	27.5	27.5	25.0	25.0
parameters	217	614	559	1229
H-atom treatment	constrained to parent site	constrained to parent site	constrained to parent site	constrained to parent site
$R[F^2>2\sigma(F^2)]$, $wR(F^2)$	0.042, 0.089	0.042, 0.128	0.042, 0.082	0.090, 0.275
$\Delta\rho_{max}$, $\Delta\rho_{min}$ [e Å^{-3}]	0.63, −0.41	0.58, −0.78	0.52, −0.49	1.00, −0.73
CSD numbers[b]	632818	632819	632820	632821

[a] All samples were measured using $Mo_{K\alpha}$ radiation (0.71075 Å), scan mode ω, at 150 K. All structures were solved by direct methods using SHELXS, and full-matrix least-squares refinements on F^2 were carried out using SHELXL. Computer programs: Bruker SMART version 5.624 or 5.625 (Bruker, **2001**); Bruker SAINT version 6.02a or 6.36a (Bruker, **2000**); Bruker SHELXTL (Bruker, **2001**); SHELXS-97 (Sheldrick, **1990**); SHELXL-97 (Sheldrick, **1997**); enCIFer (Allen et al., **2004**); PLATON (Spek, **2003**). [b] CCDC-623813–623821 contain the supplementary crystallographic data for this paper. These data can be obtained free of charge from the Cambridge Crystallographic Data Centre via www.ccdc.cam.ac.uk/data_request/cif.

$H_4L^5(TsOH)_4$: Dialdehyde **ii** (0.200 g, 0.565 mmol), 4,5-dimethyl-1,2-diaminobenzene (0.061 g, 0.565 mmol) and HOTs·H_2O (0.430 g, 2.26 mmol) were combined; yield 49%. ^{1}H NMR ([D$_6$]DMSO): δ_H=8.76 (br s, 4H, imine), 7.53–7.35 (m, 24H, arylsulfonyl+aryl+pyrrole), 7.17–7.00 (m, 20H, arylsulfonyl+aryl+pyrrole), 2.27 ppm (s, 24H, Me arylsulfonyl+Me); this complex proved too insoluble for a $^{13}C\{^1H\}$ NMR spectrum to be recorded; elemental analysis calcd (%) for $C_{90}H_{84}N_8O_{12}S_4$: C 67.65, H 5.30, N 7.01; found: C 67.03, H 4.99, N 6.87.

Synthesis of the neutral macrocycles H_4L: A solution of the tosylic salt $H_4L(TsOH)_4$ in warm (ca. 50°C) methanol was treated with a large excess of NEt_3 (ca. 1 mL), causing the immediate loss of orange colour and deposition of a voluminous yellow precipitate in all cases. The solids were collected on a glass frit, washed with methanol (3×10 mL) and Et_2O (3×5 mL) and dried at 10^{-2} mbar/50°C for 2 h.

H_4L^1: Yield 95%. ^{1}H NMR ($CDCl_3$+[D$_4$]methanol): δ_H=8.07 (s, 4H, imine), 7.06 (m, 8H, H aryl), 6.50 (d, 4H, $J_{H,H}$=3.7 Hz, pyrrole), 5.97 (d, 4H, $J_{H,H}$=3.7 Hz, pyrrole), 3.60 (br s, 4H, pyrrole NH), 1.79 ppm (s, 12H, Me); $^{13}C\{^1H\}$ NMR ($CDCl_3$, [D$_4$]methanol): δ_C=148.4 (s, imine), 146.2 (s, quaternary), 145.1 (s, quaternary), 129.8 (s, quaternary), 126.0 (s, CH), 117.7 (s, CH), 117.1 (s, CH), 106.7 (s, CH), 36.0 (s, quaternary), 27.3 ppm

(s, Me); IR (KBr): $\tilde{\nu}$ = 3395, 2972, 2874, 1624, 1560, 1469, 1429, 1369, 1264 cm^{-1}; UV/Vis ($CHCl_3$): λ_{max} (ε) = 345 (75812); ES-MS: *m/z* (%): 606 [M^++1] (100); elemental analysis calcd (%) for $C_{38}H_{36}N_8$: C 75.47, H 6.00, N 18.53; found: C 75.28, H 5.80, N 18.34.

H_4L^2: Yield 97%. ^{1}H NMR ($CDCl_3$): δ_H = 8.12 (s, 4H, imine), 6.85 (s, 4H, aryl), 6.49 (d, 4H, J_{HH} = 2.5 Hz, pyrrole), 6.06 (d, 4H, $J_{H,H}$ = 2.5 Hz, pyrrole), 2.25 (s, 12H, Me), 1.84 ppm (s, 12H, Me); $^{13}C\{^1H\}$ NMR ($CDCl_3$): δ_C = 147 (s, imine), 145.1 (s, quaternary), 143.0 (s, quaternary), 134.4 (s, quaternary), 130.7 (s, quaternary), 118.6 (s, CH), 116.4 (s, CH), 106.2 (s, CH), 35.8 (s, quaternary), 27.5 (s, Me), 19.4 ppm (s, Me); ES-MS: *m/z* (%): 660 [M^++1] (100); elemental analysis calcd for $C_{42}H_{44}N_8$: C 76.33, H 6.71, N 16.96; found: C 76.16, H 6.54, N 17.16.

H_4L^3: Yield 93%. Crystals suitable for X-ray crystallography were obtained by slow evaporation of a solution of H_4L^3 in EtOH. ^{1}H NMR ($CDCl_3$/[D_4]methanol): δ_H = 8.22 (s, 4H, imine), 7.21 (m, 4H, aryl), 7.39 (s, 4H, aryl), 7.23 (m, 4H, aryl), 6.58 (d, 4H, $J_{H,H}$ = 3.69 Hz, pyrrole), 6.01 (d, 4H, J_{HH} = 3.69 Hz, pyrrole), 1.83 ppm (s, 4H, CH_3); $^{13}C\{^1H\}$ ($CDCl_3$/[D_4]methanol): δ_C = 159.1 (s), 152.8 (s), 141.6 (s), 136.5 (s), 131.2 (s), 126.6 (s), 125.6 (s), 121.4 (s), 119.0 (s), 107.8 (s), 43.4 (s), 33.1 (s), 30.2 ppm (s); IR (KBr): $\tilde{\nu}$3401, 3325, 3049, 2969, 2874, 1607, 1559, 1579, 1489, 1449, 1365, 1270, 1234, 1212, 1171, 154, 1040 cm^{-1}; ES-MS: *m/z* (%): 705 [M^++1] (100); elemental analysis calcd for $C_{46}H_{40}N_8$: C 78.38, H 5.72, N 15.90; found: C 78.06, H 6.37, N 15.74.

H_4L^4: Yield 95%. ^{1}H NMR ($CDCl_3$): δ_H = 8.09 (s, 4H, imine), 7.00–7.32 (m, 28H, aryl), 6.50 (d, 4H, $J_{H,H}$ = 3.7 Hz, pyrrole), 5.80 ppm (d, 4H, $J_{H,H}$ = 3.7 Hz. pyrrole); $^{13}C\{^1H\}$ NMR ($CDCl_3$): δ_C = 151.8 (s, imine), 144.8 (s, quaternary), 144.7 (s, quaternary), 131.3 (s, CH), 129.7 (s, CH), 127.9 (s, CH), 127.3 (s, CH), 125.9 (s, CH), 120.6 (s, quaternary), 117.3 (s, quaternary), 113.5 (s, CH), 56.6 ppm (s, quaternary); ES-MS: *m/z* (%): 853 [M^++1] (100); elemental analysis calcd for $C_{58}H_{44}N_8$: C 81.66, H 5.20, N 13.14; found: C 81.53, H 5.31, N 13.22.

H_4L^5: Yield 97%. ^{1}H NMR ($CDCl_3$): δ_H = 8.08 (s, 4H, imine), 7.31–7.22 (m, 12H, aryl), 7.07–7.04 (m, 8H, aryl), 6.81 (s, 4H, aryl), 6.48 (d, 4H, $J_{H,H}$ = 3.7 Hz, pyrrole), 5.88 (d, 4H, $J_{H,H}$ = 3.7 Hz, pyrrole), 2.23 ppm (s, 12H, Me); $^{13}C\{^1H\}$ NMR ($CDCl_3$): δ_C = 150.8 (s, imine), 144.6 (s, quaternary), 142.6 (s, quaternary), 140.4 (s, CH), 134.1 (s, quaternary), 131.3 (s, CH), 129.5 (s, CH), 127.7 (s, CH), 127 (s, CH), 121.7 (s, quaternary), 116.54 (s, CH), 113.2 (s, CH), 56.4 (s, quaternary), 19.7 ppm (s, Me); ES-MS: *m/z* (%): 909 [M^++1] (100); elemental analysis calcd for $C_{62}H_{52}N_8$: C 81.91, N 5.77, N 12.33; found: C 82.03, H 5.88, N 12.44.

Synthesis of 1,1-bis(2-pyrrolyl)-3,3,5,5-tetramethylcyclohexane (DPM^{Cy}): Pyrrole (40 mL, 346 mmol) was briefly degassed under a stream of N_2 with constant stirring, then 3,3,5,5-tetramethylcyclohexanone (5 mL, 29 mmol) was added. As soon as a catalytic amount of trifluoroacetic acid was added, a golden colouration of the reaction mixture was observed. Stirring was continued overnight to give a greenish solution. After neutralisation with 0.1 M NaOH (10 mL), the mixture was extracted into EtOAc (50 mL); the organic phase was then washed with water (3× 20 mL) and dried over Na_2SO_4. Subsequent removal of the solvent in vacuo and trituration of the resulting viscous oil in pentane afforded crude **DPM^{Cy}** as a grey-green powder. Column chromatography (SiO_2, EtOAc/hexane 1:4, R_f = 0.71) afforded 4.24 g, 55% of **DPM^{Cy}** as a colourless oil that crystallised on cooling to −20 °C. ^{1}H NMR (270 MHz, C_6D_6): δ_H = 7.05 (s, 2H, NH), 6.10 (m, 4H, pyrrole C*H*), 6.00 (m, 2H, pyrrole CH), 1.70 (s, 4H, cyclohexyl CH_2), 1.0 (s, 2H, cyclohexyl CH_2), 0.82 ppm (s, 12H, cyclohexyl CH_3); EIMS (+ve mode): *m/z* (%): 271 [*M*+H] (48), 205 [*M*−pyrrole] (60).

Synthesis of 1,1-bis(4-formylpyrrol-2-yl)-3,3,5,5-tetramethylcyclohexane (iii): $POCl_3$ (2 mL, 21.5 mmol) was added dropwise to a stirred solution of **DPM^{Cy}** (2.65 g, 9.8 mmol) in DMF (25 mL) at 0 °C causing a deep cherry red solution to form. The mixture was stirred for 4 h at RT, after which the solution was once more cooled with an ice bath and the reaction quenched by dropwise addition of H_2O (80 mL). Aqueous KOH (2 M) was then added dropwise until the solution became strongly basic and colourless solids precipitated. The solids were collected by filtration, washed with water (2×15 mL) and dried under vacuum to yield 2.74 g, 85.8% of **iii** as a colourless powder. ^{1}H NMR (300 MHz, $CDCl_3$): δ_H = 10.7 (br, NH, 2H), 9.34 (s, CHO, 2H), 6.80 (m,, 2H pyrrole CH), 6.14 (m, 2H, pyrrole CH), 2.17 (s, 4H, cyclohexyl CH_2), 1.19 (s, 2H, cyclohexyl CH_2), 0.89 ppm (s, 12H, cyclohexyl CH_3); $^{13}C\{^1H\}$ NMR ($CDCl_3$): δ_H = 178.2 (CHO), 146.4 (*C*CHO), 131.1 (quaternary pyrrole C), 121.5 (pyrrole CH), 107.6 (pyrrole CH), 50.6 (cyclohexyl CH_2), 44.5 (cyclohexyl CH_2), 38.7 (*meso* C), 31.7 (cyclohexyl CH_3), 30.6 ppm (quaternary cyclohexyl C); ES-MS (+ve mode, MeOH): *m/z* (%): 327.20 (100) [*M*+H], 349.19 (41) [*M*+Na], 653.40 (38) [2*M*+H], 675.39 (24) [2*M*+Na]; elemental analysis calcd (%) for $C_{20}H_{26}N_2O_2$: C 73.6, H 8.0, N 8.6; found: C 73.5, H 7.8, N 8.6.

Synthesis of macrocycle H_4L^6: A mixture of **iii** (1.40 g, 4.28 mmol) and *o*-phenylenediamine (0.46 g, 4.28 mmol) in methanol was warmed until most of the solids had dissolved, giving a pale yellow suspension. A solution of TFA (0.98 g, 8.56 mmol) in MeOH (5 mL) was slowly added, causing the entire residual solid to dissolve and yielding a bright red solution. The mixture was stirred for 30 min and the solvents were removed under vacuum to afford $H_4L^6.(CF_3COOH)_4$ as a bright red solid. ES-MS (+ve mode, MeOH): *m/z* (%): 797.50 (24) [*M*+H], 843.50 (87) [*M*+H+2Na]; elemental analysis calcd (%) for $C_{60}H_{64}N_8O_8F_{12}$: C 57.5, H 5.1, N 8.9; found: C 57.6, H 5.2, N 8.8. This solid was then redissolved in MeOH (20 mL) and warmed slightly. An excess of a saturated solution of KOH in MeOH was added causing a bright yellow solid to precipitate. The solid was then collected by filtration and washed with cold MeOH (5 mL), water (until the washings were neutral) and finally pentane (10 mL), and dried under vacuum to yield 0.98 g, 57.7% of H_4L^6. Single crystals suitable for X-ray diffraction were grown by slow evaporation of a Et_2O solution. ^{1}H NMR (300 MHz, $CDCl_3$): δ_H = 8.07 (s, 4H, imine CH), 7.04 (m, 8H, phenyl), 6.40 (s, 4H, pyrrole CH), 6.00 (s, 4H, pyrrole CH), 1.98 (br s, 8H, CH_2), 1.19 (s, 4H, CH_2), 0.88 ppm (s, 24H, CH_3); $^{13}C\{^1H\}$ NMR ($CDCl_3$): δ_C = 151 (Ar*C*−N=), 144.5 (−*C*HN=), 130 (pyrrolic quaternary *C*), 125.8 (aromatic CH), 120 (aromatic CH), 117.2 (pyrrole CH), 107 (pyrrole CH), 52 (cyclohexyl CH_2), 46 (cyclohexyl CH_2), 40 (*meso* C), 32.8 (cyclohexyl CH3), 31.7 ppm (quaternary cyclohexyl C). One quaternary pyrrole C not observed.

Synthesis of palladium(II) complexes: A stirred solution of H_4L in CH_2Cl_2 (15 mL) was treated with a solution of $Pd(OAc)_2$ (2 equiv) in CH_2Cl_2 (10 mL). The resultant mixture was stirred for 0.5 h at room temperature, after which the solids had dissolved, and then treated with NEt_3 (ca. 0.2 mL). The resulting deep red solution was stirred for 16 h, reduced in volume and the crude product precipitated by addition of Et_2O or Et_2O/pentane. Recrystallisation from CH_2Cl_2/Et_2O resulted in the desired complexes of acceptable purity.

[$Pd_2(L^1)$]: H_4L^1 (0.135 g, 0.288 mmol) and $Pd_2(OAc)_2$ (0.100 g, 0.445 mmol) were combined; yield 78%. ^{1}H NMR ($CDCl_3$): δ_H = 7.23 (s, 4H, imine), 6.77 (m, 4H, aryl), 6.72 (d, 4H, $J_{H,H}$ = 3.9 Hz, pyrrole), 6.62 (m, 4H, aryl), 6.17 (d, 4H, $J_{H,H}$ = 3.9 Hz, pyrrole), 1.60 (s, 6H, CH_3), 1.50 ppm (s, 6H, CH_3); $^{13}C\{^1H\}$ NMR ($CDCl_3$): δ_C = 159.3 (s, imine), 152.7 (s, quaternary), 142.8 (s, quaternary), 136.5 (s, quaternary) 126.1 (s, CH), 124.1 (s, CH), 118.8 (s, CH), 107.7 (s, CH), 43.3 (s, quaternary), 33.1 (s, CH_3), 30.3 ppm (s, CH_3); IR (KBr): $\tilde{\nu}$ = 3442, 3088, 2966, 2924, 1557, 1502, 1473, 1445, 1390, 1327, 1263, 1196 cm^{-1}; UV/Vis ($CHCl_3$): λ_{max} (ε): 311 (36293), 414 (22256), 433 nm (22205); ES-MS: *m/z* (%): 812 [M^+ +1] (100); elemental analysis calcd (%) for $C_{38}H_{32}N_8Pd_2$: C 56.10, H 3.96, N 13.77; found: C 56.34, H 4.12, N 14.01.

[$Pd_2(L^2)$]: H_4L^2 (0.100 g, 0.151 mmol) and $Pd_2(OAc)_2$ (0.068 g, 0.302 mmol) were combined; yield 68%. ^{1}H NMR ($CDCl_3$): δ_H = 7.29 (s, 4H, imine), 6.78 (d, 4H, $J_{H,H}$ = 3.9 Hz, pyrrole), 6.53 (s, 4H, aryl), 6.23 (d, 4H, $J_{H,H}$ = 3.9 Hz, pyrrole), 2.10 (s, 12H, Me), 1.67 (s, 6H, Me), 1.60 ppm (s, 6H, Me); $^{13}C\{^1H\}$ NMR ($CDCl_3$): δ_C = 159.7 (s, imine), 152.8 (s, quaternary), 141.1 (s, quaternary), 136.9 (s, quaternary), 134.4 (s, quaternary), 125.4 (s, CH), 118.9 (s, CH), 107.9 (s, CH), 43.7 (s, quaternary), 33.1 (s, Me), 31.2 (s, Me), 19.6 ppm (s, Me); ES-MS: *m/z* (%): 871 [M^++1] (100); elemental analysis calcd (%) for $C_{42}H_{40}N_8Pd_2$: C 58.01, H 4.64, N 12.88; found: C 57.89, H 4.57, N 12.81.

[$Pd_2(L^3)$]: H_4L^3 (0.154 g, 0.218 mmol) and $Pd(OAc)_2$ (0.098 g, 0.437 mmol) were combined; yield 67% Crystals suitable for X-ray crystallography were obtained by Et_2O diffusion into a CH_2Cl_2 solution of **1c**. ^{1}H NMR ($CDCl_3$): δ_H = 7.39 (s, 4H, imine), 7.15 (m, 4H, aryl), 7.03 (m, 8H, aryl), 6.83 (d, 4H, $J_{H,H}$ = 3.9 Hz, pyrrole), 6.28 (d, 4H, $J_{H,H}$ =

3.9 Hz, pyrrole), 1.72 (s, 6H, CH_3), 1.60 ppm (s, 6H, CH_3); ^{13}C {^1H} ($CDCl_3$): δ_C = 159.1 (s), 152.8 (s), 141.6 (s), 136.5 (s), 131.2 (s), 126.6 (s), 125.6 (s), 121.4 (s), 119.0 (s), 107.8 (s), 43.4 (s), 33.1 (s), 30.2 ppm (s); IR (KBr): $\tilde{\nu}$3442, 3051, 2966, 1561, 1473, 1456, 1392, 1330, 1263, 1208, 1079, 1047 cm^{-1}; ES-MS: *m/z* (%) 915 [M^++1] (100), 899 [M^+−CH_3] (50); elemental analysis calcd (%) for $C_{46}H_{36}N_8Pd_2$: C 60.47, H 3.97, N 12.26; found: C 60.34, H 3.86, N 12.10.

[Pd_2(L^4)]: H_4L^4 (0.100 g, 0.117 mmol) and $Pd_2(OAc)_2$ (0.053 g, 0.235 mmol) were combined; yield 82%. ^1H NMR ($CDCl_3$): δ_H = 7.33 (s, 4H, imine), 7.26–6.98 (m, 10H, aryl phenyl), 6.86 (m, 4H aryl), 6.79 (m, 4H, aryl), 6.69 (d, 4H, $J_{H,H}$ = 3.9 Hz, pyrrole), 5.89 ppm (d, 4H, $J_{H,H}$ = 3.9 Hz, pyrrole); $^{13}C\{^1H\}$ NMR ($CDCl_3$): δ_C = 159.9 (s, imine), 151.1 (s, quaternary), 146.1 (s, quaternary), 142.2 (s, quaternary), 137.2 (s, CH), 129.4 (s, CH), 129.0 (s, CH) 127.8 (s, CH), 127.7 (s, CH), 126.5 (s, quaternary) 126.2 (s, quaternary), 126.0 (s, CH), 124.0 (s, CH), 119.0 (s, CH) 112.5 (s, CH), 62.4 ppm (s, quaternary); ES-MS: *m/z* (%): 1064.4 [M^++1] (100); elemental analysis calcd (%) for $C_{58}H_{40}N_8Pd_2$: C 65.61, H 3.80, N 10.55; found: C 62.66, H 3.57, N 9.76.

[Pd_2(L^5)]: H_4L^5 (0.100 g, 0.110 mmol) and $Pd_2(OAc)_2$ (0.049 g, 0.220 mmol) were combined; yield 78% ^1H NMR ($CDCl_3$): δ_H = 7.32 (s, 4H, imine), 7.28–7.23 (m, 15H, aryl), 7.08–7.02 (m, 15H, aryl), 6.68 (d, 4H, $J_{H,H}$ = 3.9 Hz, pyrrole), 6.63 (s, 4H, aryl), 5.88 (d, 4H, $J_{H,H}$ = 3.9 Hz, pyrrole), 2.12 ppm (s, 12H, Me); $^{13}C\{^1H\}$ NMR ($CDCl_3$): δ_C = 159.8 (s, imine), 150.8 (s, quaternary), 146.3 (s, quaternary), 139.97 (s, CH), 137.2 (s, CH), 134.0 (s, CH), 129.4 (s, CH), 129.0 (s, CH), 127.7 (s, CH), 127.6 (s, CH), 126.3 (s, quaternary), 126.1 (s, quaternary), 124.8 (s, CH), 118.5 (s, CH), 112.2 (s, CH), 62.3 (s, quaternary), 19.1 ppm (s, CH_3); ES-MS: *m/z* (%): 1118 (100) [M^++1]; elemental analysis calcd (%) for $C_{62}H_{48}N_8Pd_2$: C 66.61, H 4.33, N 10.02; found: C 66.45, H 4.27, N 10.12.

Synthesis of nickel(II) complexes: A stirred solution of H_4L in CH_2Cl_2 (15 mL) (H_4L^1 forms a slurry) was treated with a solution of $NiCl_2{\cdot}6H_2O$ (2 equiv) in methanol (ca. 5 mL). The mixture was allowed to stir at room temperature for 1 h before the addition of Et_3N (ca. 0.5 mL). The resultant deep red solution was stirred for a further 15 h, after which the solvents were evaporated under vacuum and the residue washed with water (25 mL). The solids were isolated by suction filtration, washed with water (2×25 mL), dried at 10^{-2} mbar/50 °C for 2 h and recrystallised from MeOH/$CHCl_3$/Et_2O.

[Ni_2(μ-OMe)$_2$$Cl_2$(HOMe)$_2$($H_4L^1$)]: H_4L^1 (0.200 g, 0.331 mmol) was combined with $NiCl_2{\cdot}6H_2O$ (0.157 g, 0.662 mmol); yield 77%. ES-MS: *m/z* (%): 792 [M^+−2MeO−2MeOH] (20), 720 [M^+−2Cl−2MeO−2MeOH] (100); elemental analysis calcd (%) for $C_{42}H_{50}Cl_2N_8Ni_2O_4$: C 54.88, H 5.48, N 12.19; found: C 54.98, H 5.37, N 12.37.

[Ni_2(μ-OH)$_2$$Cl_2$(HOMe)($H_4L^5$)]: H_4L^5 (0.200 g, 0.220 mmol) was combined with $NiCl_2{\cdot}6H_2O$ (0.104 g, 0.441 mmol); yield 89%. ES-MS: *m/z* (%): 1024 (100) [M^+−2Cl−MeOH−2OH]; elemental analysis calcd (%) for $C_{63}H_{58}Cl_2N_8Ni_2O_3$: C 65.04, H 5.02, N 9.63; found: C 65.04, H 4.85, N 9.47.

Synthesis of [Ni_2(L^1)]: A suspension of KH (0.066 g, 1.65 mmol) in THF (2 mL) was added to a stirred solution of H_4L^1 (0.20 g, 0.33 mmol) in THF (ca. 15 mL) causing rapid evolution of H_2 gas. The resultant mixture was stirred at room temperature for 1.5 h, then added to a suspension of [$NiCl_2$(dme)] (0.205 g, 0.933 mmol) in THF (20 mL), and the resultant dark brown suspension was stirred at 80 °C for 48 h during which the solution turned deep red and a pale precipitate formed. The mixture was filtered, the filtrate evaporated to dryness under vacuum and the crude red product recrystallised from toluene at −15 °C yielding 0.09 g, 19% of [Ni_2(L^1)] as red microcrystals. Crystals suitable for X-ray diffraction were obtained by cooling a saturated solution of [Ni_2(L^1)] in toluene/pentane (1/1). ^1H NMR (C_6D_6): δ_H = 6.71 (d, 4H, J_{HH} = 3.93 Hz, pyrrole), 6.64 (s, 4H, imine), 6.49 (m, 8H, aryl), 6.20 (d, 4H, $J_{H,H}$ = 3.90 Hz, pyrrole), 1.57 (s, 6H, CH_3), 1.35 ppm (s, 6H, CH_3); $^{13}C\{^1H\}$ NMR (C_6D_6): δ_C = 160.1 (s), 156.7 (s), 142.7 (s), 138.5 (s), 125.9 (s), 124.8 (s), 120.1 (s), 109.5 (s), 40.6 (s), 29.6 (s), 17.7 ppm (s); ES-MS: *m/z* (%): 705 [M^++1] (75), 661 [M^+−Ni] (100); elemental analysis calcd (%) for $C_{38}H_{32}N_8Ni_2$: C 63.56, H 4.49, N 15.60; found: C 63.43, H 4.57, N 15.56.

Synthesis of copper(II) complexes [Cu_2(L)] (L = L^1, L^2): A solution of Cu(BF_4)$_2{\cdot}H_2O$ (2 equiv) in minimal MeOH was combined with H_4L in CH_2Cl_2. After 0.5 h, an excess of NEt_3 (ca. 1 mL) was added, and the deep brown solution stirred for a further 5 h, after which the volume was reduced under vacuum and the crude material precipitated by the addition of Et_2O/pentane (1/1). The brown solids were then redissolved in $CHCl_3$ (10 mL) and washed with water (3×5 mL), dried over $MgSO_4$, filtered and evaporated to yield [Cu_2(**L**)] as brown solids.

[Cu_2(L^1)]: H_4L^1 (0.100 g, 0.166 mmol) was combined with Cu(BF_4)$_2{\cdot}H_2O$ (0.084 g, 0.354 mmol); yield 76%. UV/Vis ($CHCl_3$): λ_{max} (ε): 379 (34787), 416 nm (27195); ES-MS: *m/z* (%): 727 [M^++1] (100); μ_{eff} = 2.49 μ_B; elemental analysis calcd for $C_{38}H_{32}N_8Cu_2(C_5H_{12})$: C 64.56, H 5.54, N 14.01; found: C 65.02, H 5.62, N 13.92.

[Cu_2(L^2)]: H_4L^2 (0.200 g, 0.331 mmol) was combined with Cu(BF_4)$_2{\cdot}H_2O$ (0.143 g, 0.602 mmol); yield 87%. ES-MS: *m/z* (%) 784 [M^++1] (100); μ_{eff} = 1.99 μ_B; elemental analysis calcd (%) for $C_{42}H_{40}N_8Cu_2$: C 64.35, H 5.14, N 14.29; found: C 64.01, H 5.00, N 14.23.

[Cu_2(L^3)]: A solution of Cu(BF_4)$_2{\cdot}H_2O$ (0.076 g, 0.298 mmol) in MeOH (3 mL) was added to a stirred suspension of H_4L^3 (0.100 g, 0.142 mmol) in CH_2Cl_2 (ca. 15 mL). The resultant mixture was stirred for 20 min at room temperature, during which all the solids dissolved, and was then treated with NEt_3 (ca. 0.2 mL). The resultant dark brown solution was stirred at room temperature for 4 h, reduced in volume and crude [Cu_2(L^3)] precipitated by cooling to −15 °C. Recrystallisation from warm CH_2Cl_2 (ca. 5 mL, 40 °C) yielded 0.050 g, 43% of [Cu_2(L^3)] as purple needles. Crystals of [Cu_2(μ-py)(L^3)] suitable for X-ray crystallography were grown by Et_2O diffusion into a CH_2Cl_2/pyridine solution of [Cu_2(L^3)].

Data for [Cu_2(L^3)]: IR (KBr): ν 3418, 3083, 3051, 2967, 2919, 2853, 1564, 1500, 1465, 1386, 1315, 1264, 1205, 1067, 1044 cm^{-1}; ES-MS: *m/z* (%): 827 [M^++1] (100); μ_{eff} = 2.64 μ_B; elemental analysis calcd (%) for $C_{46}H_{36}N_8Cu_2$: C 66.73, H 4.38, N 13.53; found: C 66.78, H 4.48, N 13.63.

Data for [Cu_2(μ-py)(L^3)]: μ_{eff} = 3.09 μ_B; elemental analysis calcd (%) for $C_{51}H_{41}N_9Cu_2$: C 67.53, H 4.56, N 13.90; found: C 67.48, H 4.49, N 13.89.

Synthesis of [Mn_2(L^1)]: Toluene (15 mL) was added to a stirred mixture of [Mn(thf){N(SiMe$_3$)$_2$}$_2$] (0.300 g, 0.446 mmol) and H_4L^1 (0.174 g, 0.288 mmol). The resulting deep red solution was heated at 90 °C under partial vacuum for 12 h and, upon cooling to room temperature, deposited an amorphous red solid. The solvent was removed under vacuum to yield 0.061 g, 38% of [Mn_2(L^1)] as a rust red powder. Crystallisation of **5** by slow cooling of a hot saturated toluene solution generated [Mn_2(μ-OH)(L^1)] as dark red/brown rods. μ_{eff} = 6.97 μ_B; elemental analysis calcd (%) for $C_{38}H_{32}N_8Mn_2$: C 64.23, H 4.54, N 15.77; found: C 63.94, H 4.56, N 15.69.

Acknowledgements

The authors thank the EPSRC(UK), The Royal Society and the University of Nottingham for their support. M.S. gratefully acknowledges receipt of a Royal Society Wolfson Merit Award and of a Royal Society Leverhulme Trust Senior Research Fellowship.

[1] E. Y. Tshuva, S. J. Lippard, *Chem. Rev.* **2004**, *104*, 987.
[2] J. P. Collman, R. Boulatov, C. J. Sunderland, L. Fu, *Chem. Rev.* **2004**, *104*, 561.
[3] J. P. Collman, L. Fu, P. C. Herrmann, X. Zhang, *Science* **1997**, *275*, 949.
[4] D. J. Evans, C. J. Pickett, *Chem. Soc. Rev.* **2003**, *32*, 268; D. J. E. Spencer, A. C. Marr, M. Schröder, *Coord. Chem. Rev.* **2001**, *219–221*, 1055.
[5] M. D. Fryzuk, S. A. Johnson, *Coord. Chem. Rev.* **2000**, *200–202*, 379; B. A. MacKay, M. D. Fryzuk, *Chem. Rev.* **2004**, *104*, 385.
[6] R. H. Holm, P. Kennepohl, E. I. Solomon, *Chem. Rev.* **1996**, *96*, 2563.
[7] A. L. Gavrilova, B. Bosnich, *Chem. Rev.* **2004**, *104*, 349; M. J. McNevin, J. R. Hagadorn, *Inorg. Chem.* **2004**, *43*, 8547; J. R. Hagadorn, M. J. McNevin, G. Wiedenfeld, R. Shoemaker, *Organometallics* **2003**, *22*, 4818; G. Rowlands, *Tetrahedron* **2001**, *57*, 1865; J. Du Bois,

T. J. Mizoguchi, S. J. Lippard, *Coord. Chem. Rev.* **2000**, *200–202*, 443; E. K. van den Beuken, B. L. Feringa, *Tetrahedron* **1998**, *54*, 12985; B. Bosnich, *Inorg. Chem.* **1999**, *38*, 2554.

[8] J. L. Dempsey, A. J. Esswein, D. R. Manke, J. Rosenthal, J. D. Soper, D. G. Nocera, *Inorg. Chem.* **2005**, *44*, 6879.

[9] J. P. Collman, P. S. Wagenknecht, J. E. Hutchinson, *Angew. Chem.* ***1994****, 106*, 1620; *Angew. Chem. Int. Ed. Engl.* **1994**, *33*, 1537.

[10] C. J. Chang, Z.-H. Loh, C. Shi, F. C. Anson, D. G. Nocera, *J. Am. Chem. Soc.* **2004**, *126*, 10013; C. J. Chang, Y. Deng, C. Shi, F. C. Anson, D. G. Nocera, *Chem. Commun.* **2000**, 1355; R. Guilard, S. Brandès, C. Tardieux, A. Tabard, M. L'Her, C. Miry, P. Gouerec, Y. Knop, J. P. Collman, *J. Am. Chem. Soc.* **1995**, *117*, 11721; L. M. Proniewicz, J. Odo, J. Goral, C. K. Chang, K. Nakamoto, *J. Am. Chem. Soc.* **1989**, *111*, 2105; C. K. Chang, H. Y. Liu, I. Abdalmuhdi, *J. Am. Chem. Soc.* **1984**, *106*, 2725; R. R. Durand, Jr., C. S. Bencosme, J. P. Collman, F. C. Anson, *J. Am. Chem. Soc.* **1983**, *105*, 2710; J. P. Collman, P. Denisevich, Y. Konai, M. Marrocco, C. Koval, F. C. Anson, *J. Am. Chem. Soc.* **1980**, *102*, 6027; J. M. Hodgkiss, C. J. Chang, B. J. Pistorio, D. G. Nocera, *Inorg. Chem.* **2003**, *42*, 8270; B. J. Pistorio, C. J. Chang, D. G. Nocera, *J. Am. Chem. Soc.* **2002**, *124*, 7884; J. Rosenthal, T. D. Luckett, J. M. Hodgkiss, D. G. Nocera, *J. Am. Chem. Soc.* **2006**, *128*, 6546; J. Rosenthal, B. J. Pistorio, L. L. Chng, D. G. Nocera, *J. Org. Chem.* **2005**, *70*, 1885.

[11] J. P. Collman, H. T. Fish, P. S. Wagenknecht, D. A. Tyvoll, L.-L. Chng, T. A. Eberspacher, J. I. Brauman, J. W. Bacon, L. H. Pignolet, *Inorg. Chem.* **1996**, *35*, 6746.

[12] J. P. Collman, J. E. Hutchison, P. S. Wagenknecht, N. S. Lewis, M. A. Lopez, R. Guilard, *J. Am. Chem. Soc.* **1990**, *112*, 8206.

[13] J. P. Collman, J. E. Hutchison, M. S. Ennis, M. A. Lopez, R. Guilard, *J. Am. Chem. Soc.* **1992**, *114*, 8074; J. P. Collman, J. E. Hutchison, M. A. Lopez, R. Guilard, *J. Am. Chem. Soc.* **1992**, *114*, 8066; J. P. Collman, J. E. Hutchison, M. A. Lopez, R. Guilard, R. A. Reed, *J. Am. Chem. Soc.* **1991**, *113*, 2794.

[14] W. Cui, B. B. Wayland, *J. Am. Chem. Soc.* **2004**, *126*, 8266; W. Cui, X. P. Zhang, B. B. Wayland, *J. Am. Chem. Soc.* **2003**, *125*, 4994; X.-X. Zhang, B. B. Wayland, *Inorg. Chem.* **2000**, *39*, 5318.

[15] K. M. Kadish, L. Fremond, F. Burdet, J.-M. Barbe, C. P. Gros, R. Guilard, *J. Inorg. Biochem.* **2006**, *100*, 858; K. M. Kadish, J. Shao, Z. Ou, R. Zhan, F. Burdet, J.-M. Barbe, C. P. Gros, R. Guilard, *Inorg. Chem.* **2005**, *44*, 9023; K. M. Kadish, J. Shao, Z. Ou, L. Fremond, R. Zhan, F. Burdet, J.-M. Barbe, C. P. Gros, R. Guilard, *Inorg. Chem.* **2005**, *44*, 6744; K. M. Kadish, L. Fremond, Z. Ou, J. Shao, C. Shi, F. C. Anson, F. Burdet, C. P. Gros, J.-M. Barbe, R. Guilard, *J. Am. Chem. Soc.* **2005**, *127*, 5625; R. Guilard, F. Burdet, J.-M. Barbe, C. P. Gros, E. Espinosa, J. Shao, Z. Ou, R. Zhan, K. M. Kadish, *Inorg. Chem.* **2005**, *44*, 3972; K. M. Kadish, Z. Ou, J. Shao, C. P. Gros, J.-M. Barbe, F. Jerome, F. Bolze, F. Burdet, R. Guilard, *Inorg. Chem.* **2002**, *41*, 3990; R. Guilard, F. Jérome, C. P. Gros, J.-M. Barbe, Z. Ou, J. Shao, K. M. Kadish, *C. R. Acad. Sci. Paris* **2001**, *4*, 245; R. Guilard, F. Jerome, C. P. Gros, J.-M. Barbe, Z. Ou, J. Shao, K. M. Kadish, *C. R. Acad. Sci. Ser. IIc Chim.* **2001**, *4*, 245; R. Guilard, C. P. Gros, F. Bolze, F. Jerome, Z. Ou, J. Shao, J. Fischer, R. Weiss, K. M. Kadish, *Inorg. Chem.* **2001**, *40*, 4845.

[16] R. Guilard, F. Jerome, J.-M. Barbe, C. P. Gros, Z. Ou, J. Shao, J. Fischer, R. Weiss, K. M. Kadish, *Inorg. Chem.* **2001**, *40*, 4856.

[17] J. L. Sessler, D. Seidel, *Angew. Chem.* **2003**, *115*, 5292; *Angew. Chem. Int. Ed.* **2003**, *42*, 5134; A. Jasat, D. Dolphin, *Chem. Rev.* **1997**, *97*, 2267.

[18] W. B. Callaway, J. M. Veauthier, J. L. Sessler, *J. Porphyrins Phthalocyanines* **2004**, *8*, 1.

[19] N. N. Gerasimchuk, A. Gerges, T. Clifford, A. Danby, K. Bowman-James, *Inorg. Chem.* **1999**, *38*, 5633.

[20] W. A. Reiter, A. Gerges, S. Lee, T. Deffo, T. Clifford, A. Danby, K. Bowman-James, *Coord. Chem. Rev.* **1998**, *174*, 343.

[21] F. V. Acholla, F. Takusagawa, K. Bowman-Mertes, *J. Am. Chem. Soc.* **1985**, *107*, 6902.

[22] J. B. Love, A. J. Blake, C. Wilson, S. D. Reid, A. Novak, P. B. Hitchcock, *Chem. Commun.* **2003**, 1682.

[23] M. Taniguchi, A. Balakumar, D. Fan, B. E. McDowell, J. S. Lindsey, *J. Porphyrins Phthalocyanines* **2005**, *9*, 554; P. D. Beer, A. G. Cheetham, M. G. B. Drew, O. D. Fox, E. J. Hayes, T. D. Rolls, *Dalton Trans.* **2003**, 603.

[24] S. D. Reid, A. J. Blake, C. Wilson, J. B. Love, *Inorg. Chem.* **2006**, *45*, 636.

[25] S. D. Reid, A. J. Blake, W. Köckenberger, C. Wilson, J. B. Love, *Dalton Trans.* **2003**, 4387.

[26] G. Givaja, A. J. Blake, C. Wilson, M. Schröder, J. B. Love, *Chem. Commun.* **2003**, 2508.

[27] J. M. Veauthier, E. Tomat, V. M. Lynch, J. L. Sessler, U. Mirsaidov, J. T. Markert, *Inorg. Chem.* **2005**, *44*, 6736.

[28] J. M. Veauthier, W.-S. Cho, V. M. Lynch, J. L. Sessler, *Inorg. Chem.* **2004**, *43*, 1220.

[29] J. L. Sessler, W.-S. Cho, S. P. Dudek, L. Hicks, V. M. Lynch, M. T. Huggins, *J. Porphyrins Phthalocyanines* **2003**, *7*, 97.

[30] R. Li, T. A. Mulder, U. Beckmann, P. D. W. Boyd, S. Brooker, *Inorg. Chim. Acta* **2004**, *357*, 3360.

[31] J. L. Sessler, S. Camiolo, P. A. Gale, *Coord. Chem. Rev.* **2003**, *240*, 17.

[32] J. A. Wytko, M. Michels, L. Zander, J. Lex, H. Schmickler, E. Vogel, *J. Org. Chem.* **2000**, *65*, 8709.

[33] C. Janiak, *J. Chem. Soc. Dalton Trans.* **2000**, 3885.

[34] Y. Deng, C. J. Chang, D. G. Nocera, *J. Am. Chem. Soc.* **2000**, *122*, 410.

[35] Z.-H. Loh, S. E. Miller, C. J. Chang, S. D. Carpenter, D. G. Nocera, *J. Phys. Chem. A* **2002**, *106*, 11700.

[36] Y. Shimazaki, T. Nagano, H. Takesue, B.-H. Ye, F. Tani, Y. Naruta, *Angew. Chem.* **2004**, *116*, 400; *Angew. Chem. Int. Ed.* **2004**, *43*, 98; K. Ichihara, Y. Naruta, *Chem. Lett.* **1998**, 185; Y. Naruta, M. Sasayama, K. Ichihara, *J. Mol. Catal. A Chem.* **1997**, *117*, 115; Y. Naruta, M. Sasayama, T. Sasaki, *Angew. Chem.* **1994**, *106*, 1839; *Angew. Chem. Int. Ed. Engl.* **1994**, *33*, 1839.

[37] Y. Shimazaki, H. Takesue, T. Chishiro, F. Tani, Y. Naruta, *Chem. Lett.* **2001**, 539.

[38] G. J. Park, S. Nakajima, A. Osuka, K. Kim, *Chem. Lett.* **1995**, 255.

[39] A. Osuka, S. Nakajima, T. Nagata, K. Maruyama, K. Toriumi, *Angew. Chem.* **1991**, *103*, 579; *Angew. Chem. Int. Ed. Engl.* **1991**, *30*, 582.

[40] P. L. Arnold, A. J. Blake, C. Wilson, J. B. Love, *Inorg. Chem.* **2004**, *43*, 8206; P. L. Arnold, D. Patel, A. J. Blake, C. Wilson, J. B. Love, *J. Am. Chem. Soc.* **2006**, *128*, 9610.

[41] I. L. Eremenko, S. E. Nefedov, A. A. Sidorov, M. A. Golubnichaya, P. V. Danilov, V. N. Ikorskii, Y. G. Shvendenkov, V. M. Novotortsev, I. I. Moiseev, *Inorg. Chem.* **1999**, *38*, 3764.

[42] F. Speiser, P. Braunstein, L. Saussine, *Inorg. Chem.* **2004**, *43*, 4234.

[43] Z. Xu, L. K. Thompson, D. A. Black, C. Ralph, D. O. Miller, M. A. Leech, J. A. K. Howard, *J. Chem. Soc. Dalton Trans.* **2001**, 2042.

[44] G. Givaja, A. J. Blake, C. Wilson, M. Schroder, J. B. Love, *Chem. Commun.* **2005**, 4423.

[45] C. J. Chang, E. A. Baker, B. J. Pistorio, Y. Deng, Z.-H. Loh, S. E. Miller, S. D. Carpenter, D. G. Nocera, *Inorg. Chem.* **2002**, *41*, 3102.

[46] G. Pognon, C. Boudon, K. J. Schenk, M. Bonin, B. Bach, J. Weiss, *J. Am. Chem. Soc.* **2006**, *128*, 3488.

[47] E. M. Schubert, *J. Chem. Educ.* **1992**, *69*, 62; D. F. Evans, *J. Chem. Soc.* **1959**, 2003.

[48] E. C. Constable, A. J. Edwards, M. J. Hannon, P. R. Raithby, *J. Chem. Soc. Chem. Commun.* **1994**, 1991; E. C. Constable, T. Kulke, M. Neuburger, M. Zehnder, *Chem. Commun.* **1997**, 489; M. G. B. Drew, A. Lavery, V. McKee, S. M. Nelson, *J. Chem. Soc. Dalton Trans.* **1985**, 1771; C. Piguet, G. Bernardinelli, A. F. Williams, *Inorg. Chem.* **1989**, *28*, 2920; K. T. Potts, M. Keshavarz, F. S. Tham, H. D. Abruna, C. Arana, *Inorg. Chem.* **1993**, *32*, 4450; T. Yano, R. Tanaka, I. Kinoshita, K. Isobe, L. J. Wright, T. J. Collins, *Chem. Commun.* **2002**, 1396.

[49] C. J. Chang, Z.-H. Loh, Y. Deng, D. G. Nocera, *Inorg. Chem.* **2003**, *42*, 8262.

[50] D. Jokic, C. Boudon, G. Pognon, M. Bonin, K. J. Schenk, M. Gross, J. Weiss, *Chem. Eur. J.* **2005**, *11*, 4199; S. Yagi, M. Ezoe, I. Yonekura, T. Takagishi, H. Nakazumi, *J. Am. Chem. Soc.* **2003**, *125*, 4068.
[51] D. Sun, F. S. Tham, C. A. Reed, L. Chaker, M. Burgess, P. D. W. Boyd, *J. Am. Chem. Soc.* **2000**, *122*, 10704.
[52] R. L. Belford, N. D. Chasteen, R. E. Tapscott, *J. Am. Chem. Soc.* **1969**, *91*, 4675; J. F. Boas, R. H. Dunhill, J. R. Pilbrow, R. C. Srivastava, T. D. Smith, *J. Chem. Soc. A* **1969**, 94; J. F. Boas, J. R. Pilbrow, C. R. Hartzell, T. D. Smith, *J. Chem. Soc. A* **1969**, 572; R. H. Dunhill, J. R. Pilbrow, T. D. Smith, *J. Chem. Phys.* **1966**, *45*, 1474; R. H. Dunhill, J. R. Pilbrow, T. D. Smith, *J. Chem. Soc. A* **1968**, 2189.
[53] S. S. Eaton, K. M. More, B. M. Sawant, G. R. Eaton, *J. Am. Chem. Soc.* **1983**, *105*, 6560.
[54] S. S. Eaton, G. R. Eaton, C. K. Chang, *J. Am. Chem. Soc.* **1985**, *107*, 3177.
[55] L. Nordenskiold, A. Laaksonen, J. Kowalewski, *J. Am. Chem. Soc.* **1982**, *104*, 379.
[56] J.-M. Barbe, F. Burdet, E. Espinosa, R. Guilard, *Eur. J. Inorg. Chem.* **2005**, 1032.
[57] F. Franchesci, G. Guillemot, E. Solari, C. Floriani, N. Re, H. Birkedal, P. Pattison, *Chem. Eur. J.* **2001**, *7*, 1468; E. Gallo, E. Solari, N. Re, C. Floriani, A. Chiesi-Villa, C. Rizzoli, *Angew. Chem.* **1996**, *108*, 2113; *Angew. Chem. Int. Ed. Engl.* **1996**, *35*, 1981.
[58] H.-R. Chang, S. K. Larsen, P. D. W. Boyd, C. G. Pierpont, D. N. Hendrickson, *J. Am. Chem. Soc.* **1988**, *110*, 4565; S. Gou, Q. Zeng, Z. Yu, M. Qian, J. Zhu, C. Duan, X. You, *Inorg. Chim. Acta* **2000**, *303*, 175; N. Shaikh, A. Panja, S. Goswami, P. Banerjee, P. Vojtíšek, Y.-Z. Zhang, G. Su, S. Gao, *Inorg. Chem.* **2004**, *43*, 849.
[59] B. Horvath, R. Moeseler, E. G. Horvath, *Z. Anorg. Allg. Chem.* **1979**, *450*, 165.
[60] A. B. Pangborn, M. A. Giardello, R. H. Grubbs, R. K. Rosen, F. J. Timmers, *Organometallics* **1996**, *15*, 1518.
[61] J. L. Sessler, E. Tomat, T. D. Mody, V. M. Lynch, J. M. Veauthier, U. Mirsaidov, J. T. Markert, *Inorg. Chem.* **2005**, *44*, 2125.

Received: July 11, 2006
Revised: October 5, 2006
Published online: January 24, 2007

